

Ref. #1

First, we would like to thank the reviewer for his/her comments which have helped improving the paper and the analysis of the results.

- In general, the level of scientific writing could be improved. Please try to avoid subjective terms like 'very good' and 'extremely high' in the text.

-> We have taken care of avoiding such expressions in the revised version.

- The inventory-based comparison should be extended, since it now only focuses on GFEDv3 and MODIS BA (which is actually used in the GFEDv3 modeling framework and therefore the overlap between both datasets is not surprising at all). From a bottom-up perspective, it would be interesting to add inventories that rely on other methods as well, like e.g. the Global Fire Assimilation System (GFAS; based on fire radiative power (FRP)) and the Fire Inventory from NCAR (FINN). Extending the comparison with these inventories could give more insight in the processes that explain the discrepancy found with the diurnal cycle of IASI CO, and might bolster your hypothesis on the contribution of changes in the flaming and smoldering phase.

-> We have extended our comparisons between diurnal CO and fire products to the GFASA1.0 monthly product. In southern Africa, GFAS1.0 is lower than GFED3.1 but follows in general the same seasonal cycle (picking ~1 month earlier than the diurnal signal of CO) and agrees better with the diurnal signal of CO in terms of interannual variability. The agreement is also better in terms of spatial repartition. In the revised version, Fig.2c is plotted for both GFED3.1 and GFAS1.0: the emissions on the East of the area (35-40_E) between July and September, that are not "seen" with the diurnal signal of CO (see Section 3.2.2), are lower for GFAS1.0 than for GFED3.1. GFAS1.0 emissions are also lower in this area than the ones located between 10 and 30_E, in agreement with IASI CO signal.

This overall better agreement is illustrated by a better correlation coefficient found between GFAS1.0 and the diurnal signal of CO ($R^2 \sim 0.7$ instead of 0.6 for GFED3.1) on all the tropical regions.

The reasons why GFAS and GFED differ are certainly complex and investigating these reasons exceeds the scope of this paper. The MODIS BA have been used here to provide a more "direct" observation of the fire location. Thus, in our view, the fact that GFED uses the MODIS BA in its framework is interesting since the agreement with the diurnal CO signal should be closer to the emissions than to the BA themselves, IASI CO providing a signature of the emissions themselves. Using the MODIS BA also permits to extend the comparison to the beginning of 2012, a period that is not available from GFED3.1.

- How confident are the authors that the mechanisms described for the boreal forest fire case (P17L1-7) are valid for Africa savanna fires or deforestation fires in South America?

-> We do not (and cannot) state that the mechanisms are exactly the same. The results from Ferguson et al. (2003) stem from a punctual (in time and space) study, and depend on the weather in the studied days, the topography, etc. We draw a parallel between our two studies, supported by our findings and the evolution of the boundary layer height, which is described just after in the text.

- In contrast to the 9.30am measurements, I guess that the 9.30pm measurement can be affected by transport from other regions? If so, the diurnal cycle will be impacted by CO transport from other regions as well. An atmospheric transport model could be used to check whether transport does play a role in this diurnal cycle, or, at least, provide the reader with some references to convince that this is not the case. In general, more discussion on the role of transport is important, especially regarding the comparison of the different regions (vegetation types) in Africa. If transport does play a role, interpreting those results does not make sense.

-> Both the 9.30 a.m. and 9.30 p.m. measurements are affected by transport from other regions. When talking about the remaining high values of CO in southern Africa outside of the fire season (for example in Fig. 3), both “day” and “night” IASI CO mixing ratios are influenced by transport, and they are influenced the same way.

Concerning the effect of transport on the diurnal signal of CO, it is of course not excluded that both large scale circulation and local conditions have an influence. Rio et al. (2010) showed that the DTE of CO₂ was not always necessarily located just above the source, because of large scale advection (“ [...] the real DTE signal can be significant in surrounding areas, due to preferential directions of the large scale advections.”). Chédin et al. (2009) showed that the DTE of CO₂ could be negative on a daily scale due to particular horizontal winds. However, on a monthly basis, outside the source region, the DTE daily variations tend to cancel each other out.

A distinction should be made between the influence of large scale (and long distance) transport that affects day and night IASI CO for months, and the particular horizontal winds that can punctually affect the day minus night difference of CO.

On monthly averages, the diurnal signal of CO is thus mostly located in the vicinity of the sources and can be interpreted in relation to the region above which it is located.

This discussion has been added to the text.

- Instead of July 2008, how does the boundary layer behave in southern Africa in the months of August-November? How does the boundary layer behave in South America in the fire season?

-> The BL behaves the same way in August-November as in July, but the maximum of the height (reached at 12:00) increases from July (_2.0 km) to September (_2.5 km), and then decreases until November (1.5 km).

In South America, a similar behaviour is found (based on ECMWF forecasts), except that a lower height is reached in July-October (not higher than _1.8 km). This has been included in the revised text.

- What would be the impact of deforestation fires in South America on the diurnal CO signature of IASI? These fires are often started in the afternoon (>9.30am), and represent a significant part of CO emissions in the South American Continent. The same counts for Indonesia.

-> A diurnal signal of CO is found in South America too and it is in agreement with fire activity. It is located in the area of the “arc of deforestation” and its evolution follows the fire activity.

It is more difficult to see what would be the impact of Indonesian fires, as it is a smaller region that is affected by persistent cloudiness – few clear sky observations are available.

- Besides the fact that the diurnal CO signal may reveal some interesting findings with respect to the temporal variations in fire emissions, the method could be potentially useful above regions where other sources of pollution occur, like e.g. Asia. I'm wondering why, in the global analysis (Figure 7), Asia is left out of the analysis. Indonesia and Southeast Asia are important tropical regions from a biomass burning perspective, and given the proximity to anthropogenic pollution sources the method could be specifically useful in these regions.

-> Southeast Asia and Indonesia are smaller fire sources than Africa and South America, on which we put an emphasis. And as indicated above, we are limited by the number of clear sky observations to study these regions in details.

- I miss some discussion on how to proceed with this method in future. Are there other sensors or upcoming missions that could be used? What about sensors with surface sensitivity to CO, like MOPITT? Could the work directly be combined with CO₂ observations? In general, I miss a sort of guidance here.

-> We have added a paragraph about other and future spatial missions in the conclusion. Metop-B was launched in 2012 and Metop-C will be launched in 2017, so IASI will provide at least 20 years of observations, at the same equator crossing times, allowing us to study on the long term the evolution of CO, its diurnal cycle and its relation with fires. IASI-NG, on the same orbit, will cover the period 2020-2042.

Our CO retrieval method also works with Aqua/AIRS observations (see Thonat et al., 2012), whose passing times are 1.30 a.m./p.m. CrIs, with the same characteristics as AIRS, was launched in 2011 and will also be on the JPSS program planned for 2017.

Terra/MOPITT gives CO measurements at 10.30 a.m/p.m. So, with IASI and AIRS, it gives access to 6 points a day in the diurnal cycle of CO. However, our retrieval method cannot be applied to MOPITT, which is a different instrument from the AIRS and IASI TIR sounders, with only 8 channels located in the thermal infrared part of the spectrum, which prevents using the double spectral difference approach to derive CO columns. Having a different retrieval chain can lead to biases with our AIRS and IASI retrievals. Nonetheless, studying both TIR and TIR+NIR CO retrievals from MOPITT, which have different vertical sensitivities, can give valuable information on the vertical distribution of CO.

Since IASI enables the retrieval of other gases emitted by fires such as CO₂ or CH₄, the simultaneous study of the retrieved fields of CO and these other gases is clearly foreseen. In particular, the extension of the DTE of CO₂ to other regions and all the IASI period is currently under investigation.

Technical corrections

All technical corrections and suggestions have been taken into account in the revised paper. We just have a few remarks on the following ones.

P5L23: From a CO perspective fire emissions are not particularly strong in southern Africa. Deforestation fires in the Amazon and South-East Asia, and boreal wildfires have in general stronger smoldering components and therefore a stronger CO signal

-> According to GFED3.1, Africa (and in particular southern Africa) is a major contributor to CO fire emissions. The tropics gather 80% of fire emissions of carbon, that's why we have focused on CO retrievals in this region. Moreover, southern Africa is a region weakly affected by cloud coverage (as opposed to Southern America and South-East Asia), yielding a higher number of day and night observations.

P8L7: Why not take the average of 2007-2012 instead of 2008 only?

-> 2008 is an average year in terms of fire activity. We have checked that the conclusions do not differ when plotting the average of 2007-2012.

P11L5-6: 'The day-night signal is observed just above fires'. Is it? I'm not sure when looking at Figure 3?

-> The diurnal signal of CO can indeed be important where fires are not indicated by the MODIS BA, but the main signal is always located in their vicinity (for example it is not located over the oceans).

“The day-night is observed just above fires” has been replaced by “The day-night signal mostly captures CO over fires”.

P12L5: Looking at Figure 5, I'm not convinced that these defined regions actually capture a certain vegetation type. For example, H9 seems very heterogenic.

-> These regions were defined by Hoelzemann (2006) to study the seasonal cycle of fires between different emission inventories. Although it is not stated that this choice was made to fit to different vegetation types, she found different emission source distribution between these ten regions in terms of fuel types (see Fig. 3.9 in Hoelzemann (2006), where e.g. wildfires in H1 are dominated by forest fires, and wildfires in H9 are dominated by savanna and grassland fires). This has been specified in the revised version.

P13L26: So did you include these areas to derive the r^2 of 0.6? If not, make clear in the text.

-> Fig. 8 has been remade to fix a problem with the average computation. The conclusions are the same except it is for the entire dataset that we have $R^2 \sim 0.6$. We only mention R^2 value for the entire dataset in the revised paper. As said above, we have also specified that R^2 value is 0.7 for GFAS1.0.

P17L1-17: This is the case for a boreal fire, which is in general quite different than a savanna, cropland or tropical deforestation fire. How would the pyroconvection and natural convection work for a savanna fire in southern Africa?

-> Answering this question would require to use a pyro-thermal plume model like Rio et al. (2010) did, and it is goes beyond the subject of this paper. In the conclusion we call for such a use that could confirm our hypothesis.

Ref. #2

First, we would like to thank the referee for his/her suggestions which have helped improving the content of the paper and the analysis of the results. The answers to his/her questions are given below.

General comments

■ The influence of the thermal contrast on the sensitivity of our retrievals to CO, and, through that, its influence on the day-night difference of CO is indeed an important question. Quantifying this influence is a difficult task: our retrieval gives access to an integrated content of CO (not a profile), and without knowing the true profile of CO corresponding to the IASI overpass, we can just make a hypothesis on the mechanism explaining the diurnal signal of CO. Section 4.1 shows that the different vertical sensitivity to CO between night and day has an influence on the retrieved diurnal signal of CO. The day-night difference of $q\text{CO}^{4A}$, which only depends on the diurnal variation of the weighting function, displays almost the same seasonality as our diurnal signal of CO. However, we conclude that the impact of the vertical sensitivity is not decisive. In the revised version of the paper, we go further in the analysis of the link between the thermal contrast and our CO retrievals.

Figure A1 below shows: (i) the difference of the thermal contrast between day and night for July 2008 in southern Africa; (ii) the corresponding day-night CO. The thermal contrast over the ocean is indeed quite stable between day and night but mostly higher during daytime. On the continent the day-night difference of the thermal contrast is everywhere positive and exceeds 20 K on the West and South West of the area. The comparison between both maps of Fig. A1 reveals that diurnal signal of CO and thermal contrast have quite different spatial distributions. West and South-West of the area, the diurnal signal of CO is not at its highest; and it reaches its maximum values for an average day-night difference of the thermal contrast.

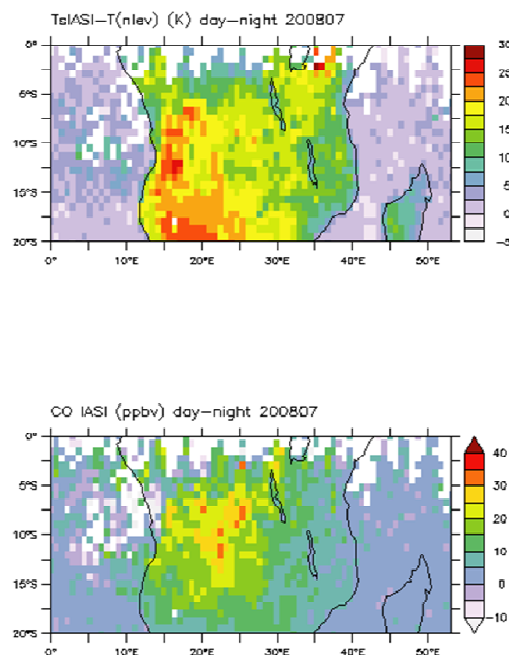


Figure A1. (top) Day-night difference of the thermal contrast in July 2008 (in K), in July 2008 in southern Africa. (bottom) Day-night difference of IASI CO (in ppbv).

This is confirmed by Fig. A2 which plots retrieved CO by day, by night and day-night, against thermal contrast, for the same area and during the fire season. A high/low thermal contrast doesn't necessarily leads to a high/low IASI CO retrieval, by day or by night. The same is true for the day-night difference of CO. Moreover, values of the diurnal signal of CO higher than 10 ppbv (red in Fig. A2c), which are the ones we are interested in since they are related to fires, correspond to a wide range of thermal contrast variations between day and night; and for these values the correlation between day-night CO and thermal contrast is weak ($R \sim 0.2$).

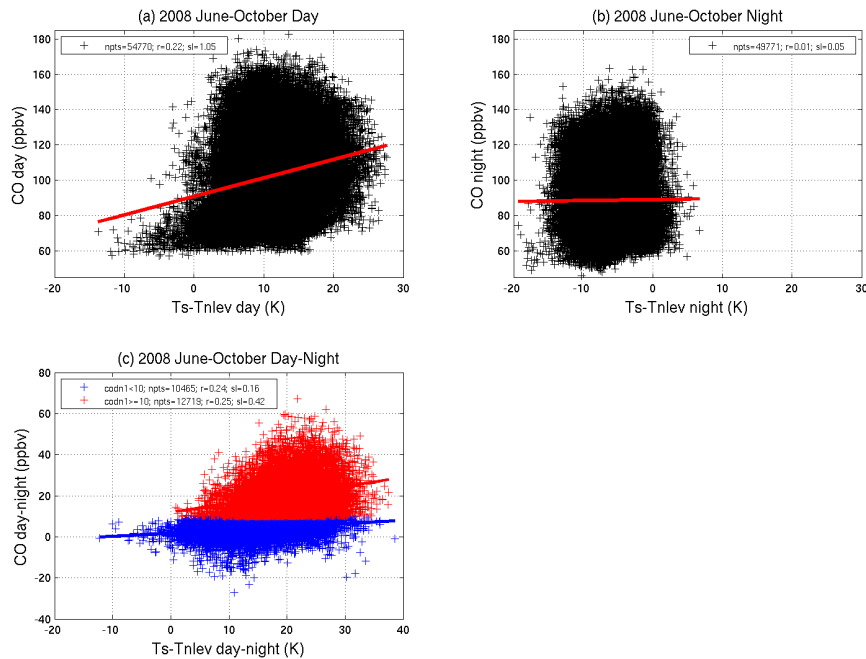


Figure A2. (a) IASI CO (in ppbv) by day as a function of the thermal contrast (in K), between June and October 2008, in southern Africa, on land. (b) Same as (a), by night. (c) Same as (a), for the day-night difference. Values of day-night CO higher than 10 ppbv are displayed as red crosses, whereas values lower than 10 ppbv are plotted in blue.

■ In section 4.1, we study the influence of the weighting function on the retrieved diurnal signal of CO via the day-night difference of qCO^{4A} . Given that qCO^{4A} is the product of the weighting function and the input profile in 4A, and that only one input profile is used, the day-night difference of qCO^{4A} only depends on the variation of the weighting function. The first part of this response showed that there was no clear correlation between the thermal contrast and the diurnal signal of CO. This second part is a discussion on the meaning of the day-night difference of qCO^{4A} .

Figure A3 shows, for July 2008 in southern Africa, maps of the day-night difference of: (i) (total) CO, (ii) qCO^{4A} , (iii) ΔqCO and (iv) thermal contrast. The day-night difference of qCO^{4A} is very uniform in the area, where most values are comprised between 0 and 10 ppbv. ΔqCO , which may also be impacted by the thermal contrast, has a completely different spatial distribution from qCO^{4A} . So, although the day-night difference of qCO^{4A} is a component of the retrieved day-night difference of CO, it mostly plays the role of a bias and does not introduce any geographical pattern seen in day-night CO.

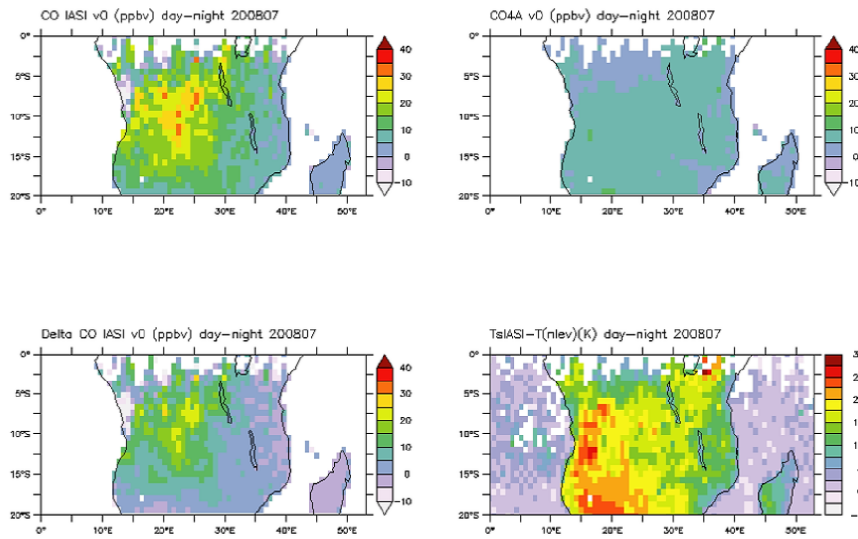


Figure A3. (top left) Day-night difference of IASI CO (in ppbv), in July 2008 in southern Africa. (top right) Day-night difference of qCO^{4A} (see text in section 4.1) (in ppbv). Day-night difference of ΔqCO (in ppbv). (bottom right) Day-night difference of the thermal contrast (in K).

The input profile in 4A corresponds to average CO conditions. In order to see what would be the effect of the variation of the vertical sensitivity with a more polluted profile, we use a modified profile in 4A, the ‘v1’ CO profile plotted in Fig. A4, which is characterized by a string excess of CO near the surface.

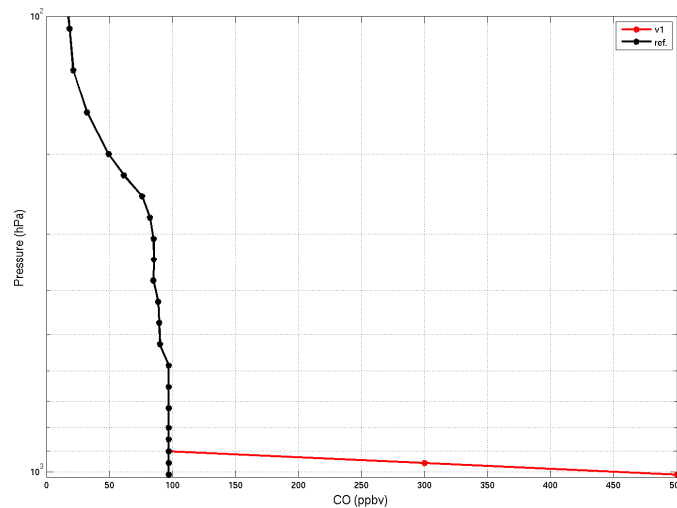


Figure A4. Black: reference profile of CO used as input in 4A for the retrieval of IASICO (in ppbv). Red: a polluted profile in the boundary layer.

First, it is worth noting that the CO retrievals computed with the v1 CO profile as input in 4A are very close to the ones computed with the reference profile, by day, by night, and also for the day-night difference of CO. This shows that our retrieval method is lowly dependent on this input variable.

Figure A5 is similar to Fig. A3 but with all 4A computations made with the v1 CO profile. The day-night difference of qCO^{4A} is still very uniform but a little higher than with the reference profile: the mean difference is 1 ppbv with a SD of 2 ppbv. Other modified profiles

have been used, with different repartitions of CO along the first layers of the troposphere: despite the fact that the day-night difference of $q\text{CO}^{4A}$ could have higher values, its distribution is always quite uniform. The day-night total CO always displays the same geographical patterns, which gives confidence in this signal.

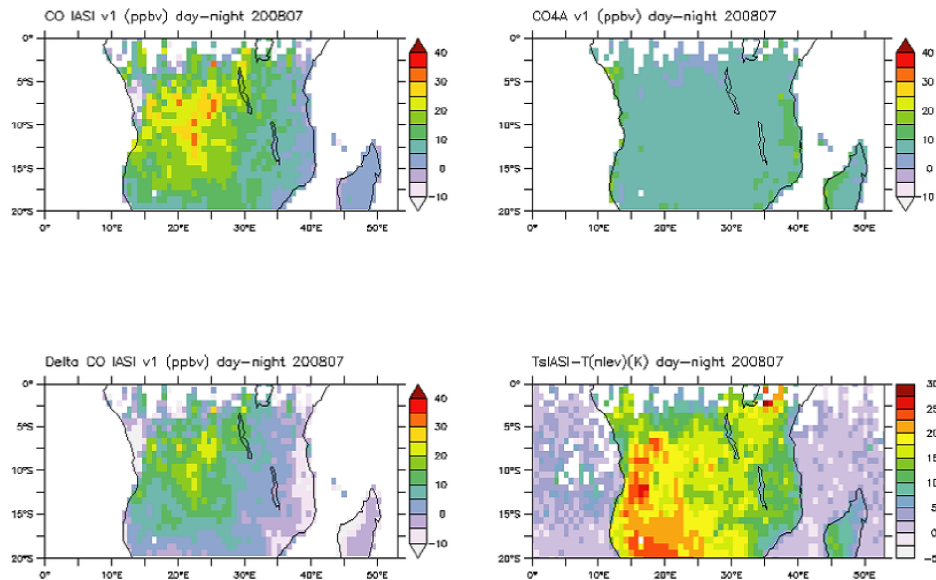


Figure A5. Same as Fig. A3, with the polluted profile 'v1' (see Fig. A4) used as input in 4A.

Figure A6 is similar to Fig. 10 in the paper, but it also shows the values of the day-night difference of $q\text{CO}^{4A}$ computed with the v1 CO profile (blue points). Due to the heavy computations requested to process the whole time series, we only plotted here 4 points in January and 4 points in July. As expected from above discussion, the day-night difference of $q\text{CO}^{4A}$ obtained with the v1 profile is higher than with the reference profile. However, it is still low compared to the diurnal signal of CO. More importantly, the amplitude of the signal has not changed. This suggests that the amplitude of 15 ppbv found for the diurnal signal of CO is not decisively influenced by the variations of the vertical sensitivity.

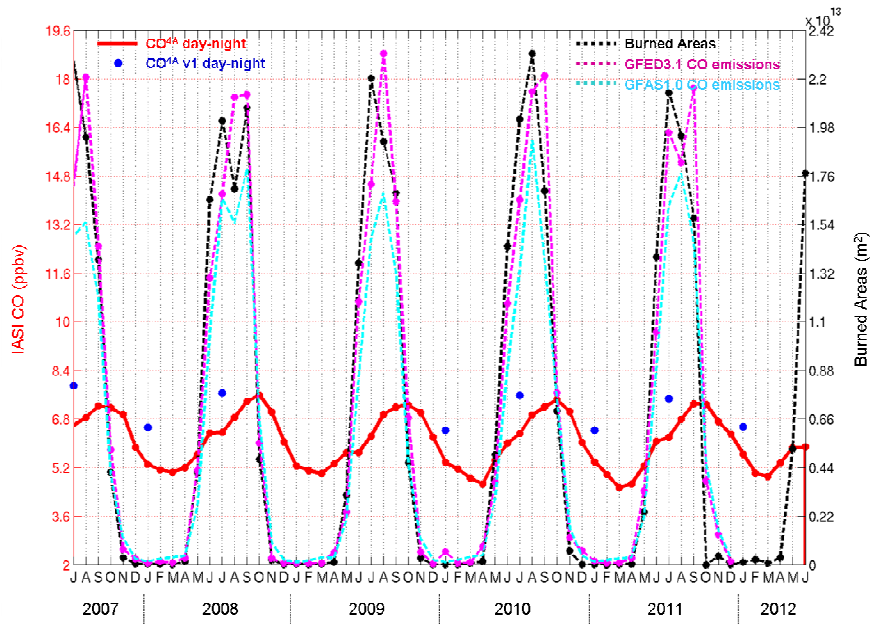


Figure A6. Evolution of the day-night difference of the integrated content qCO^{4A} on land, and of fires, between July 2007 and June 2012 in southern Africa. Red: day-night difference of qCO^{4A} . Blue dots: day-night difference of qCO^{4A} computed with the v1 CO profile as input in 4A. Black dashed: MODIS BA. Purple dashed: GFED3.1 CO emissions. Cyan dashed: GFAS1.0 CO emissions.

Section 4.1 has been extended in the revised version to take these new elements of discussion into account.

Specific comments

1. Page 26009 and Figure 1. If I understand it correctly, you use model temperatures from ECMWF but retrieve the surface temperature. I would like to see show maps of thermal contrasts (for day and night) in parallel to the CO distributions in Figure 1. This would be helpful also for analysing the results.

-> The required maps are provided as Fig. A7 below. They will be provided as supplementary material. Their use in the analysis of the retrieved CO columns is not straightforward. Basically, it can be seen that the regions characterized by high values of CO, or high values of the diurnal CO signal do not display strong thermal contrast conditions. Usually, the thermal contrast is positive during the day and negative during the night. The effect of the thermal contrast on the day and night weighting functions is already seen in Fig. 9.

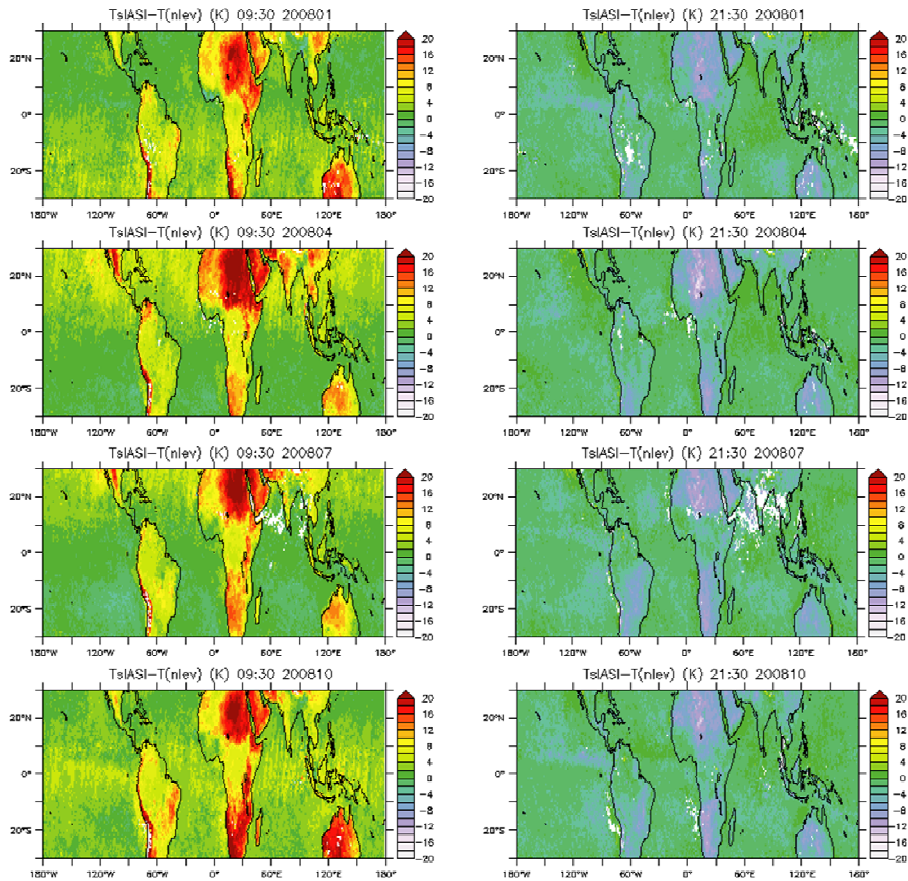


Figure A7. $T_s - T_{\text{first_layer}}$ (in K), by day (left) and by night (right), from January, April, July and October 2008. T_s comes from IASI, $T_{\text{first_layer}}$ comes from ECMWF reanalysis.

2. Section 3.2.1. and Figure 2 (also for the other Figures): Please specify how the averages have been performed, both for the total columns and for the difference: what is gridding? Do you consider per grid cell daily means from which you compute the difference (in each cell)? It is for these reasons unclear why the difference (Figure 2d) contains so many gaps. That is important also for the discussion per region in section 3.2.3. Note that Figure 2 is too small and blurry. Lat/long (mentioned in the text) are unreadable.

-> Gridding has been specified in section 3.1 and 3.2.1, and the way the difference is made has also been described a little more in section 3.2.2. The monthly mean of the day-night difference of CO is computed as follows: first the 0.75×0.75 daily means of the clear-sky retrievals of CO made at 9:30 a.m. and 9:30 p.m. are calculated; then, for each grid cell, the difference between 9:30 a.m. and 9:30 p.m. is computed for each day and averaged over the whole month.

IASI orbits by day and night hardly, if not never, cross each other near the equator. In July for example, the number of day-night differences used to compute the monthly mean (at the scale of a $0.75^\circ \times 0.75^\circ$ pixel) ranges from 1 around 2°S to 15 around 20°S . During the wet season (i.e. from November to March), the number of points available to compute the monthly mean of day-night CO is also limited by the number of clear-sky observations available.

In Fig. 6 (Section 3.2.3), areas H1 and H2 are never totally covered; in addition, the monthly means in these areas are calculated from the few days where the day-night difference of CO is available. We have added to Fig. 2 maps of the number of days from which the monthly mean has been calculated. This will also help the discussion in Section 3.2.3.

3. In section 3.3 (page 26016, line 1) you mention a correlation coefficient of 0.6. Do I get it right that this is by excluding the two regions AfsE and AmC? If yes it should be made clearer in the abstract and in the conclusion (26020, line 13) that the 0.6 correlation coefficient is not considering the entire dataset (and it would in fact be good to give the value for the entire dataset as well).

-> Fig. 8 has been remade to fix a problem with the average computation. The conclusions are the same except it is for the entire dataset that we have $R^2 \sim 0.6$. We only mention R^2 value for the entire dataset in the revised paper. As suggested by referee 1, we have also extended the comparison to the GFAS1.0 dataset: R^2 reaches 0.7 for GFAS1.0, highlighting a better agreement with IASI day-night CO.

4. Section 4.2. The fact that the CO_2 and CO day-night differences exhibit opposite signs is surprising. The proposed mechanisms could indeed lead to this but even if the smoldering phase emits more CO than CO_2 , the flaming phase is still expected to release significant amounts of CO, which would follow the same uplift mechanism as that proposed for CO_2 . Why are these enhancements not better seen in the IASI CO data? Or would this mean (again supposing that the proposed diurnal cycle is real) that the CO excess from the mid-troposphere is underestimated (as a significant fraction of CO in the upper troposphere would have been subtracted)?

-> CO and CO_2 are both emitted and uplifted during the day, during the flaming phase of the combustion, with the approximate following repartition of emissions: 90% of carbon emissions is CO_2 and 10% is CO; but our hypothesis is that the CO that is uplifted after the night (i.e. after the smoldering phase has released large quantities of it, but almost no CO_2) is more important.

Technical corrections

All technical suggestions have been taken into account in the text. We just have a few remarks on the followings.

6. Page 26009, line 16. What is meant with “A negative thermal contrast has symmetric effects”? Temperature inversions also increase sensitivity significantly.

-> The sentence has been changed: “A negative thermal contrast, on the contrary, decreases the sensitivity near the surface.” (See Fig. 2 and 3 in Thonat et al., 2012.)

7. Page 26010, line 5: Is it sound to use the term mid-tropospheric CO considering the possible impact of the sensitivity to the lowest layers? Furthermore, “tropospheric CO” is used in other occasions (e.g. in the abstract). I would suggest being homogeneous in the notations throughout, to define clearly these terms and verify that they are consistent with what is actually measured.

-> The sensitivity to CO in the mid-troposphere has been defined more precisely in Section 2.2. The reference to the mid-troposphere remains only to characterize the maximum of the sounder’s sensitivity to CO, its sensitivity to CO at night and the emissions of CO. Otherwise we now always use “tropospheric CO”.

9. Page 26013, line 5-6. *“The daytime signal is observed just above the fire”*. Are you referring here to the spatial location (in which case this is optimistic – see general comment 2) or to the better match is the maxima of the CO excess as compared to the emissions (From Figure 4)?

-> The diurnal signal of CO can indeed be important where fires are not indicated by the MODIS BA, but the main signal is always located in their vicinity (for example it is not located over the oceans). *“The day-night is observed just above fires”* has been replaced by *“The day-night signal mostly captures CO over fires”*.

10. Page 26013, line 10: *Where is transport from the NH seen? Is it not too far South to be affected by NH transport?*

-> In this period (November-April), sources are only located in the North and the high concentrations of CO in the studied area are only found near the equator.

Signature of tropical fires in the diurnal cycle of tropospheric CO as seen from Metop-A/IASI

T. Thonat^{*}, C. Crevoisier, N. A. Scott, A., Chédin, R. Armante, and L. Crépeau

Laboratoire de Météorologie Dynamique, CNRS, IPSL, Ecole Polytechnique, Palaiseau, France

[*Now at School of Geosciences, University of Edinburgh, Edinburgh, United Kingdom](#)

Abstract. Five years (July 2007-June 2012) of CO tropospheric columns derived from the IASI hyperspectral ~~infrared sounder~~[Infrared Atmospheric Sounding Interferometer \(IASI\)](#) onboard Metop-A are used to study the impact of fires on the concentrations of CO in the ~~mid-~~troposphere. Following Chédin et al. (2005, 2008), who ~~showed the existence of a found a quantitative relation between the~~ daily tropospheric excess of CO₂ ~~quantitatively related to and~~ fire emissions, we show that tropospheric CO also displays a diurnal signal with a seasonality that ~~is in very good agreement~~[agrees well](#) with the seasonal evolution of fires given by ~~GFED3.1~~[\(Global Fire Emission Database version 3 \(GFED3.1\) and Global Fire Assimilation System version 1 \(GFAS1.0\) emissions, and MODIS](#) (Moderate Resolution Imaging Spectroradiometer) [\(MODIS\) Collection 5](#) burned area ~~product~~. Unlike ~~daytime~~ or nighttime CO fields, which mix local emissions with nearby emissions transported to the region of study, the day-night difference of CO allows to highlight the CO signal due to local fire emissions. A linear relationship ~~is found in the whole tropical region~~ between CO fire emissions from the ~~GFED3.1 inventory and GFAS1.0 inventories~~ and the diurnal difference of IASI CO ~~was found over various regions in the tropics, with a better agreement with GFAS1.0 (correlation coefficient of $R^2 \sim 0.7$) than GFED3.1 ($R^2 \sim 0.6$).~~ Based on the specificity of the two main phases of the combustion (flaming vs. smoldering) and on the vertical sensitivity of the sounder to CO, the following mechanism is proposed to explain such a CO diurnal signal: at night, after the passing of IASI at 9:30 p.m. ~~LT~~[\(local time \(LT\)\)](#), a large amount of CO emissions from the smoldering phase is trapped in the boundary layer before being uplifted the next morning by natural and pyro-convection up to the free troposphere, where it is seen by IASI at 9:30 a.m. LT. The results presented here highlight the need for ~~developing complementary approaches to bottom-up emissions inventories and for~~ taking into account the specificity of both the flaming and smoldering phases of fire emissions in order to fully take advantage of CO observations.

1 Introduction

~~By combining human and natural components, biomass~~[Biomass](#) burning plays an important and singular role in the global carbon cycle, ~~with a combination of human and natural drivers~~. Fire emissions are ~~indeed~~ a major source of carbon in the atmosphere, particularly in the forms of carbon dioxide (CO₂) and carbon monoxide (CO). ~~Global emissions can vary significantly from year to year~~. According to van der Werf et al. (2010), ~~the mean global emission~~ in the 1997-2009 period ~~is up to 2.0~~, ~~they have varied between 1.5 and 3 PgC.yr⁻¹~~. ~~Global emission estimates can also differ from one inventory to another: for the year 2000 for example, Ito and Penner (2004) evaluated them at 1.4 PgC while Schulz et al. (2008) made the estimate of 2.3 PgC. On average between 1997 and 2009, the emissions are up to 2 PgC.yr⁻¹ (van der Werf et al., 2010).~~ This represents the equivalent of about one third of the total anthropogenic emissions related to fossil fuel combustion and cement production (IPCC, 2007). These global emissions are not in total a net contribution to the atmosphere since the

carbon released is partly recaptured by photosynthesis during the consecutive growth of plants. Nonetheless, they are important enough to be the main factor driving the variability of the CO₂ growth rate (Lagenfelds et al., 2002). The influence of fires on climate occurs in several ways: they have an impact on the components of radiative forcing and globally reinforce climate change (Bowman et al., 2009); they globally reduce surface albedo by producing soot; they release various chemical compounds which can reach the free troposphere (Lavoué, 2000) and then be transported around the globe (e.g., Freitas et al., 2006; Guan et al., 2008) and affect the atmospheric chemistry; aerosols emitted by fires can modify cloud coverage and precipitation patterns (Andreae, 1991; Andreae et al., 2004). However, despite their magnitude, current estimates of fire emissions of gases and aerosols still remain affected by large uncertainties.

Throughout the years, several fire emission inventories have been built based on various approaches (e.g., Hoelzemann et al., 2004; Jain et al., 2006; Lehsten et al., 2009; van der Werf et al., 2010). Most of them rely on the following equation to compute fire emissions:

$$M = A \times B \times e \times EF \quad (1)$$

where M (g) is the product of the burned areas A (m²), the biomass density B (g.m⁻²), the combustion efficiency e (g.g⁻¹) and the emission factor EF which depends on the studied gas (Seiler and Crutzen, 1980). A is generally determined from observations from space, B and e are generally given by a biogeochemical model and EF is calculated empirically, mainly based on field measurements. However, large uncertainties affect each term of this equation, meaning that these inventories alone are not sufficient to determine all the characteristics of fires and their emissions.

More recently, the GFAS 1.0 (Global Fire Assimilation System) emissions inventory (Kaiser et al., 2012) was built without using Eq. 1. It is based on the relation between the fire radiative power (FRP) and fire emissions themselves. All fuels release approximately the same quantity of energy per mass unit. Assuming that the fire radiative energy (FRE) is proportional to the total energy released by a fire, it is possible to estimate the quantity of burned biomass. Wooster et al. (2005) have shown that there was a linear relation between the FRE and the mass of burned fuels, and found a universal conversion factor. Estimates relying on this method are not dependant on the terms A , B and e of Eq. 1. However, uncertainties remain in the measure of the FRP from polar satellites, in the determination of the emission factors and in the estimation of the conversion factor (e.g., Freeborn et al., 2008) and its dependence on the vegetation type.

A more direct measure from space, which is by nature global and continuous, of biomass burning carbon emissions themselves, and more particularly of CO₂ and CO, could in principle allow us to avoid these difficulties and provide an indispensable complement to the inventories. Several studies have relied on CO observation observations from space, mostly from thermal infrared (TIR) sounders, to quantify fire emissions. Indeed, since fires emit large amount of CO in the atmosphere far above its background level, CO is known as a good proxy of fire emissions. For example, continuous CO measurements, in particular with the MOPITT (Measurements of Pollution in the Troposphere (MOPITT)) instrument, have been compared to chemistry-transport simulations based on fire emission inventories (e.g., Turquety et al., 2007; Yurganov et al., 2008). AIRS (Atmospheric Infrared Sounder (AIRS)) was the first instrument to provide daily global measurements of CO, highlighting the large-scale transport of fire emissions (McMillan et al., 2005, 2008). Observations from the more recent IASI (Infrared Atmospheric Sounding Interferometer) instrument (Hilton et al., 2012) have also been used, for example to retrieve CO fire emissions in Greece in 2007, showing

~~their undervaluation in the GFED2 (Global Fire Emission Database) inventory (Turquety et al., 2009), or to~~ study extreme fire events in Russia in 2010 (Yurganov et al., 2011) ~~or in Greece in 2007, where GFED2 (Global Fire Emission Database) emissions were shown to be undervalued (Turquety et al., 2009).~~ CO is a good indicator of fire activity, but it only represents a small fraction of the emissions, which is mostly representative of the smoldering phase of the combustion (Lobert and Warnatz, 1993). Therefore CO₂, which represents the majority of the emissions, mostly representative of the flaming phase of the combustion, has also been studied in relation with fire activity, despite the difficulty of both retrieving CO₂ from space and capturing the “fire signal” in its tropospheric concentration.

A ~~new~~ approach developed by ~~Chedin~~ Chédin et al. (2005, 2008) allows to isolate CO₂ fire emissions from space, by calculating the difference between CO₂ retrieved by night and CO₂ retrieved by day that results from the diurnal cycle of fires (Giglio, 2007). This difference is calculated from the observations of ~~TOVS~~ (TIROS-N Operational Vertical Sounder (TOVS)) onboard NOAA10 and is called Daily Tropospheric Excess (DTE). It can reach several ppmv (parts per million by volume) over regions affected by fires. The seasonal and interannual variabilities of the DTE are in agreement with ~~the ones of~~ burned areas and fire emissions, showing that there is an excess of CO₂ in the troposphere above burned areas at 7:30 p.m., few hours after the peak of fire activity, compared to the CO₂ level at 7:30 a.m.. The DTE was shown to be quantitatively related to CO₂ fire emissions in the tropics. The mechanism explaining the observation of such a signal is as follows: (i) in the afternoon, during the period of high fire activity, large quantities of CO₂ are emitted into the free troposphere; (ii) CO₂ accumulates under the tropopause and is seen by the satellite at 7:30 p.m.; (iii) CO₂ is then diluted by large-scale transport during the 12 hours preceding the next pass of the satellite, at 7:30 a.m., before fires start again. ~~Rio et al. (2010) confirmed~~ This result was theoretically ~~this result confirmed~~ with a pyro-thermal plume model (Rio et al., 2010).

As Metop passing times are 9:30 a.m./p.m., i.e. before and after the maximum of the diurnal cycle of fires, IASI is well suited to complete the study of the diurnal cycle of fire emissions initiated with TOVS. The main difficulty of the DTE remains in the retrieval of CO₂ and the weakness of the CO₂ fire signal. On the contrary, the impact of fires on the concentration of CO can be more than 100% of its background level (e.g., Turquety et al., 2009), ~~making it easier to measure~~ ~~providing a clearer signal with respect to fires~~. For these reasons, our study focuses on CO, and particularly on its diurnal variation in relation to fire activity. Our study focuses on ~~the tropics, where the majority of fire emissions are located, during the 5 years between 2007 and tropical biomass burning regions in the years 2007-2012.~~ Section 2 describes the data and the method used to retrieve CO from the IASI observations. Section 3 presents the IASI retrievals, by day and by night, in comparison with fire activity. We first focus on southern Africa, where fire emissions are particularly strong, and then on ~~the whole tropical region~~ ~~various regions in the tropics~~. Section 4 is a discussion on why the diurnal difference of CO is in better agreement with fire activity than the daytime or nighttime concentrations. Section 5 concludes this study.

2 Data and method

2.1 IASI

The Infrared Atmospheric Sounding Interferometer (~~IASI~~) is a polar-orbiting nadir-viewing instrument that measures infrared radiation emitted from the Earth. IASI is a high resolution

Fourier Transform Spectrometer based on a Michelson Interferometer, which provides 8461 spectral samples, ranging from 645 cm^{-1} to 2760 cm^{-1} ($15.5\text{ }\mu\text{m}$ and $3.6\text{ }\mu\text{m}$), with a spectral sampling of 0.25 cm^{-1} , and a spectral resolution of 0.5 cm^{-1} after apodisation (“Level 1c” spectra). IASI cross track scanning is of 2200 km [at the surface](#), allowing global coverage twice a day. The instantaneous field of view is sampled by 2x2 circular pixels whose ground resolution is 12 km at nadir. IASI was developed by the Centre National d’Etudes Spatiales (CNES) in collaboration with the European Organisation for the Exploitation of Meteorological Satellites (EUMETSAT); it was launched in October 2006 onboard the polar-orbiting Meteorological Operational Platform (Metop-A), and is operational since July 2007. In this study, use is made of the Level 1c data (available from the Ether Centre for Atmospheric Chemistry Products and Services website: <http://ether.ipsl.jussieu.fr/>, via EUMETCAST).

2.2 Retrieval [Method](#)

The retrieval scheme is based on the double difference approach described in Thonat et al. (2012), which takes advantage of the high spectral resolution of IASI. It relies on the idea of using a difference in brightness temperature (BT) between two channels having the same sensitivities to every atmospheric and surface variable but CO. This difference is thus only sensitive to CO variations and cancels out the signals coming from interfering variables (surface temperature and emissivity, temperature, water vapour and nitrous oxide). In order to interpret this BT difference in terms of CO, we use the difference between the BT simulated by the 4A (Automatized Atmospheric Absorption Atlas) (Scott and Chédin, 1981; <http://ara.abct.lmd.polytechnique.fr/>) radiative transfer model and the observed BT. The double difference then provides the amount of CO in the troposphere which is in excess (or deficit) in comparison with the a priori CO profile used as input in 4A.

For the simulated BT, use is made of [the European Centre for Medium-Range Weather Forecasts \(ECMWF\) ERA-INTERIM Reanalyses](#) as atmospheric data input to 4A. These are profiles of temperature, water vapour and ozone characterized by a 6-hour time resolution and a $0.75^\circ \times 0.75^\circ$ space resolution, colocalised in time and space to IASI clear-sky fields of view and inter/extrapolated on the 4A pressure levels. The surface temperature is estimated directly from one IASI channel (at 2501.75 cm^{-1}) to avoid the lag between the closest reanalyses and the IASI passing. The same a priori CO profile is used for every simulation. For observed BT, clouds and aerosols are detected with several threshold tests based on IASI and AMSU observations (Crevoisier et al., 2003, Pierangelo et al., 2004).

The retrieved CO column is representative of the mid-troposphere, with a maximum sensitivity at about 450 hPa, [and half a maximum between about 200 hPa and 750 hPa](#), depending on the difference between surface temperature and above air temperature: the higher this difference, [which is defined as the “thermal contrast”](#), the higher the sensitivity to CO in the lower layers of the troposphere. A negative thermal contrast [has symmetric effects, on the contrary, decreases the sensitivity near the surface](#). The retrieval method also gives access to the precision, which is about 2.5 ppbv.

CO retrievals from IASI have been compared with the CARIBIC (Civil Aircraft for the Regular Investigation of the Atmosphere Based on an Instrument Container) (Brenninkmeijer et al., 2007) aircraft measurements. The difference between CARIBIC and IASI CO is on average 3.6 ppbv, with a standard deviation of 13.0 ppbv. This [good](#) agreement is also found

above deserts and mountainous areas, highlighting that the retrievals are not impacted by surface characteristics (Thonat et al., 2012).

5 | 3 The diurnal variation of mid-IASI tropospheric CO

3.1 IASI day~~time~~ and nighttime CO over the tropics

10 | Five whole years of clear-sky observations from the IASI hyperspectral infrared sounder between July 2007 and June 2012 have been interpreted in terms of mid-tropospheric CO column, in the tropics (30°N - 30°S , ~~30°N~~), by day and night (9:30 a.m./p.m. LT (local time)). Maps of monthly means of CO in the troposphere are plotted in Fig. 1 on a $0.75^{\circ}\times 0.75^{\circ}$ grid, for January, April, July and October 2008, over land and over sea. Blank areas denote an absence of retrievals due to persistent cloudiness or aerosols. According to Fig. 1, the distribution and the seasonality of CO retrieved by day and by night are the same similar,
15 | though with lower maximum values in the nighttime.

20 | Extreme Highest CO concentrations (superior to ~ 110 ppbv) are localised above continents, in the Northern Hemisphere (NH) during the boreal winter and in the Southern Hemisphere (SH) during the austral winter. These extreme values, that concern primarily Africa and South America, stem from important biomass burnings events in the local dry season (Duncan et al., 2003). Fires are not the only source of CO in the tropics; for example high CO values are seen in China outside of the fire season, caused by a continuous pollution coming from fossil fuel combustion (industry, transport) (Buchwitz et al., 2007; Streets et al., 2006).

25 | The repartition of CO seen in Fig. 1 is also influenced by the seasonal variation of the OH radical, the main sink of CO (Holloway, 2000). During the boreal winter, OH concentrations are low in the North and high in the South (Spivakovsky et al., 1990), allowing CO emitted by fires and human activities to accumulate in the NH (Duncan et al., 2007). The opposite
30 | happens during the winter in the SH, where the anthropogenic emissions play a less important role.

High CO concentrations are also seen over sea because of the transport from continental sources. Indeed, in the mid-troposphere, where IASI retrievals are most sensitive to CO
35 | (~ 450 hPa), stronger winds and a longer lifetime of CO than at the surface make the transport of CO over long distances possible.

40 | Even if the signature of fire emissions on tropospheric CO fields is well seen, the existence of other sources than fires and the transport of fire emissions by atmospheric circulation make the study of the relation between fires and CO concentrations difficult. In order to
| enhance highlight the links between fire activity and tropospheric CO, we now take advantage of the availability provided by infrared sounders to retrieve CO both by day and night.

3.2 A case study: diurnal variation of CO over southern Africa

45

3.2.1 IASI day~~time~~ and nighttime CO

50 | We now focus our study in on southern Africa (between 0° - 20°S and 0° in latitudes, and 0° and 53°E in longitudes) since) which is an important region from a biomass burning is particularly strong in this region perspective. Moreover, as opposed in contrast to northern

Africa, southern Africa is rather preserved from strong pollution and dust events (Engelstaedter et al., 2006).

~~Figures 2a and b~~ The first two lines of Fig. 2 show the monthly means of the integrated content of CO from IASI between January and December 2008, by day (9:30 a.m.) and night (9:30 p.m.), on a 0.75°x0.75° grid. The same spatio-temporal distribution of CO is seen on both time series. However, values of IASI CO by day are stronger than the ones by night. During the dry season, there is an excess of CO shifting progressively from the North-West in May to the South and South-East until November. This excess of tropospheric CO reaches a maximum in September-October. This evolution can be explained by the evolution of fires (Cahoon et al., 1992 ; Barbosa et al., 1999) ; it is similar to the evolution of the burned areas (BA) observed by MODIS (Moderate Resolution Imaging Spectroradiometer) (MODIS) (Collection 5, Roy et al., 2008) (Fig. 2e, 4th line), as well as the evolution of fire emissions from GFED3.1 (Fig. 2, 5th line) and from GFAS1.0 (Fig. 2, 6th line), but with a shift of one to two months depending on the fire product considered. In addition, the excesses of CO in the troposphere are not located exactly above the burned areas, highlighting the transport of the CO emitted by fires, by convection and general atmospheric circulation.

The 2-months lag between the day/night retrieved CO and fires is observed for each of the 5 years studied here, as shown in Fig. 3, which represents the evolution of the monthly means of IASI CO by day and night, MODIS BA and CO emissions from GFED3.1 and GFAS1.0, in the same region as Fig. 2. It is worth noting that there are also disagreements between MODIS BA and GFED3.1 and GFAS1.0 emissions concerning the evolution of fires during the dry season. For example, according to GFED3.1, the maximum of the emissions generally occurs a month after the maximum of the burned areas. GFAS1.0 is lower than GFED3.1 and has a different interannual variability. These discrepancies are due to the fact that the emissions are not proportional to the burned areas and that many other variables are taken into account in their calculation have to be considered, like the type of vegetation, the combustion efficiency or the emission factor.

In April, which is a month of transition between the dry season in the North and the dry season in the South, IASI CO is minimum; it starts to increase in May, at the beginning of the fire season. In September-October, the maximum of the CO mixing ratio in the troposphere corresponds to the maximum of the GFED fire emissions in 2008 and 2011 but is one to two months delayed in the other years. In November, although fires are hardly active according to the MODIS BA and GFED3.1 and GFAS1.0, values of CO are still quite remain high.

Between December and ~~February~~ March, i.e. outside of the fire season in the SH, high CO values are in general still quite high found between 0° and 5°S for both day and night. This is due to the southward transport of CO emitted by northern fires and pollution. Such atmospheric processes complicate the analysis of the CO fields retrieved from space observations and our ability to disentangle the CO directly emitted by fire over the region of interest from the background and transported CO from nearby regions. This is why, following Chédin et al. (2005), we now focus on the analysis of the day-night difference of CO.

3.2.2 Day-night difference of IASI CO

Monthly means of day-night differences of CO are plotted in Fig. 2d. The day-night difference-2 (3rd line). It is calculated-out-of-computed as follows: first the 0.75°x0.75° daily means of the clear-sky retrievals of CO made at 9:30 a.m. and 9:30 p.m. are

5 calculated; then, for each grid cell, the exact same day difference between 9:30 a.m. and 9:30 p.m. is computed for every day when both daytime and nighttime retrievals are available, and then averaged over the whole month. Blank areas on the maps of Fig. 2d are due to a lack of points caused by the presence of clouds or aerosols, or. The number of points available to compute the monthly means of day-night CO is plotted in Fig. 2 (7th line). It shows that IASI orbits by day and night hardly, if not never, cross each other near the equator. During the wet season (i.e. from November to March), the number of points available to compute the monthly mean of day-night CO is also limited by the fact that the daytime and the nighttime orbits of the sounder do not overlap over these areas. number of clear-sky observations available.

10 The 5 years evolution of the monthly means of the day-night differences of CO in southern Africa, along with the evolution of MODIS BA and, GFED3.1 and GFAS1.0 emissions, are plotted in Fig. 4.

15 Unlike In contrast to the evolution of daytime and nighttime CO (Fig. 3), the temporal evolution of the diurnal difference is in very good agreement agrees well with fire activity. The maps of the diurnal difference show a positive signal between May and October which can exceed 40 ppbv. The day-night signal is observed just above mostly captures CO above fires, and follows their evolution between May and September, shifting towards South and South-East, with a maximum in September, at the same time as for the emissions, or one month later. Between November and April, i.e. outside of the fire season, although the values of CO retrieved either by day or by night are quite high because of the transport from the NH, the day-night difference of CO is almost null. Over sea, the day-night difference is null. This shows that the chosen differential approach emphasizes the CO emitted by fires while cancelling out the background CO stemming from CO emitted in other regions and then transported over the region of interest.

20 Despite this good agreement between IASI
30 The retrieved diurnal CO (Fig. 2d) signal can be affected by both large scale circulation and local conditions. Concerning the DTE of CO₂, Rio et al. (2010) showed that it was not always necessarily located just above the source, because of large scale advection, with the real DTE signal sometimes being significant in surrounding areas, due to preferential directions of the large scale advections. The DTE of CO₂ can be negative on a daily scale due to particular horizontal winds. However, on a monthly basis, outside the source region, the DTE daily variations tend to cancel each other out. A distinction should thus be made between the influence of large scale (and long distance) transport that affects day and night IASI CO for months, and the particular horizontal winds that can punctually affect the day minus night difference of CO. On monthly averages, the diurnal signal of CO is mostly located in the vicinity of the sources and can be interpreted in relation to the region above which it is located.

35 Despite the good agreement between IASI diurnal CO and fire activity given by GFED3.1, GFAS1.0 emissions and MODIS burned areas (Fig. 2e), there are some discrepancies can be found between the two of them. For instance, between July and September, the day-night difference of IASI CO between 35°E and 40°E is low despite high level of burned areas seen by MODIS. In addition Conversely, in October, the diurnal difference is very high large even though fires are very weak low. The decrease of the signal takes place a little bit diurnal signal happens later than the one decrease of fires fire activity; the signal is still important in
40 November in 2010 and 2011 albeit fires are not active any more according to MODIS and

5 | ~~GFED3.1~~the fire products (Fig. 4). This kind of discrepancy in seasonality with an emission inventory has already been observed for this area with GFED2 (Edwards et al., 2006 ; van der Werf et al., 2006 ; Roberts et al., 2009). This lag could be due to the burning of woody fuels towards the end of the dry season, that may not be well represented in the inventory. These dense fuels emit large amounts of CO and are likely to burn on a long period. After the peak of the fire season, the smoldering phase of the combustion, which is characterized by thermodynamical conditions of higher moisture and lower temperature, favours CO emissions (Lobert and Warnatz, 1993) in fires that may not be captured in terms of burned area or FRP from space observations because of their small energy.

10 | 3.2.3 Relation between the day-night difference of CO and fire emissions

15 | To study in more details the diurnal cycle of CO in southern Africa and its relation with fires in more details, we focus on several areas represented in Fig. 5a, whose coordinates are given in Table 1. These areas, adapted from Hoelzemann (2006), correspond to different kindsemission source distributions, which can be linked to the different types of vegetation, which are also represented in Fig. 5b, ~~adapted. 5,~~ taken from Mayaux et al. (2003). The dominant types in southern Africa are forests, savannas and croplands. On these areas, we calculate the mean of the day-night difference of the integrated content of CO from IASI, whose evolution is represented in Fig. . 6, on average between 2008 and 2011. Also plotted are the MODIS BA ~~and,~~ the GFED3.1 and GFAS1.0 emissions for the same period.

25 | There is a very goodgeneral agreement between the monthly evolution of the day-night difference of CO and the one of fire emissions for most of the selected areas. It is clearly visible for areas H4 and H6, concerning both the seasonality and the intensity of the signals. For areas H7 and H8, dominated by grasslands, there is a good agreement in the seasonality but the amplitude of the day-night CO is strong whereas GFED and GFAS fire emissions and MODIS BA are low. On the contrary, for H9, an area dominated by croplands, the day-night CO is lower than the GFED3.1 signal, but fits GFAS1.0. H10, Madagascar, is characterized by ~~an~~ almost nullno fire activity; as a result the day-night CO is low and constant, in agreement with the MODIS BA ~~and the,~~ GFED3.1 and GFAS1.0 emissions.

35 | According to MODIS BA ~~and,~~ GFED3.1 and GFAS1.0 emissions, areas H3 and H5 are those where fires are the most activefire activity is observed. They are also the ones for which the day-night difference of CO is the strongest. Like As for the fire season, the increase in the diurnal signal of CO begins in May. However the maximum is reached one month later than the maximum of the emissions, and high values remain until October although fires are not active any more according to the twothree fire products. The lag between the diurnal variation of CO and the two fire products observed over the whole southern Africa (cf. section 3.2.2), thus only takes place in these two areas mostly occupied by forests and wooden savannas.

45 | Areas H1 and H2, in the North of the region, display the worst agreement: the background level of the diurnal signal is quite high and there is a shift of one month of the seasonality compared to fires. ~~But~~However, as seen in Fig. 2, these areas are only havecovered by a few points available to calculate, and the monthly means in these areas are calculated from the few days where the day-night difference of CO, ~~as explained above, and as seen in Fig. 2d is~~ available.

50 | To conclude, the agreement in seasonality and intensity between fire activity and the diurnal cycle of CO in southern Africa shown in Fig. 4 is the result of an agreement between these

signals at finer scales, ~~corresponding which correspond~~ to different kinds of vegetation. ~~This agreement concerns the seasonality of the signals as well as their intensity, even though discrepancies~~ Discrepancies arise in some areas, which can be related to the specificity of CO emissions according to the kind of vegetation, and to the lack of observations available to compute a significant day-night difference of CO.

3.3 Link between day-night CO and fire emissions in the whole tropical region tropics

We now extend our study to the whole tropical zone, which is divided into 12 areas plotted in Fig. 7 and defined in Table 2. These areas are taken from Chédin et al. (2008) and are representative of the different fire seasons. Figure 8 compares the annual means of the day-night difference of CO (in ppbv) with the annual means of the GFED3.1 and GFAS1.0 emissions (in $\text{gCO}\cdot\text{m}^{-2}$), averaged over 2008-2011. ~~The GFED3.1 emissions are arbitrarily multiplied by a constant factor (found to be equals to 16) in order to “reconcile” the units.~~ Figure 8 It can be compared to Fig. 11 from Chédin et al. (2008) that shows the annual GFED2 CO₂ emissions as a function of the DTE of CO₂ computed from the TOVS observations.

A
Both with GFED and GFAS, a linear relationship can be seen between the two variables over a large interval, between 23 and 12-15 ppbv. This relationship supports the interpretation of the day-night difference of CO as a signal directly related to biomass burning emissions. Two areas set apart: GFAS1.0 displays a better agreement with the diurnal signal of CO than GFED3.1, mainly because of lower emissions in the South-East Africa (AfSE) area (see also the area H9 in Fig. 6). Otherwise, two areas set apart: North-East and Central Africa (AfNEC), with a low diurnal signal, and Central America (AmC), with a high diurnal signal, compared to the emissions. Except/Despite these two areas, the correlation is high between the diurnal signal of CO on the one hand, and the GFED3.1 emissions ($R^2 \sim 0.6$); however $R^2 \sim 0.6$) and the GFAS1.0 emissions ($R^2 \sim 0.7$) on the other hand. However it is lower than the correlation between the DTE of CO₂ and the emissions found by Chédin et al. (2008) ($R^2 \sim 0.8$).

As stressed by Chédin et al. (2008) for CO₂, the discrepancies between the emissions and the diurnal signal in the troposphere can be related to the atmospheric transport of the emissions or to complex diurnal cycles of the emissions. They also may come from a mischaracterisation of the specificity of CO emissions in fire inventories, especially from the smoldering fire phase, in GFED3.1. In particular, most of GFED3.1 emission factors are based on averages per biome that do not take into account temporal and spatial variability, although they are influenced by several environmental factors.

4 Discussion

4.1 Impact of the vertical sensitivity of the sounder on the day-night difference of CO

As seen in Fig. 4 (or Fig. 6), the diurnal excess of CO is still positive outside of the fire season, even if it stays low. Given that there is no other significant diurnal source of CO in southern Africa, these signals can be explained by the diurnal variation of the vertical sensitivity of the CO retrieval. As seen in Fig. 9, which represents the IASI CO weighting

functions in southern Africa, the weighting functions during daytime display a higher sensitivity to CO close to the surface, due to a higher thermal contrast (i.e. the difference between the surface temperature and the temperature of the first pressure level), during and outside of the fire season (July and January, respectively) (Thonat et al., 2012).

However, the comparison between both monthly maps of thermal contrast conditions and CO day-night differences over southern Africa in July 2008 (Fig. S1) reveals that diurnal signal of CO and thermal contrast have quite different spatial distributions. On the continent, the day-night difference of the thermal contrast is everywhere positive and exceeds 20 K on the West and South West of the area, where the day-night CO is not at its highest. And the day-night CO reaches its maximum values for an average day-night difference of the thermal contrast.

This result is confirmed by Fig. 10, which represents scatter plots of the thermal contrast and IASI retrievals, spot by spot, for daytime observations, nighttime observations, and for the day-night difference, between June and October 2008 in southern Africa. A high/low thermal contrast doesn't necessarily leads to a high/low IASI CO retrieval, by day or by night. The same is true for the day-night difference of CO, even though the thermal contrast is generally higher in the daytime than in the nighttime. Moreover, values of the diurnal signal of CO higher than 10 ppbv, which are the ones that are mostly related to fires, correspond to a wide range of thermal contrast variations between day and night; and for these values the correlation is weak ($R \sim 0.3$).

As was explained in section 2.2, the retrieved tropospheric column of CO qCO is the sum of the integrated content of the input profile of the radiative transfer model 4A and of the excess (or deficit) of CO estimated in respect to it. This means:

$$qCO = qCO^{4A} + \Delta qCO \quad (2)$$

The first term of this sum is given by:

$$qCO^{4A} = \sum_{i=1}^{42} wp_i \times profileCO_i^{4A} \quad (3)$$

where i is the number of the pressure layer, wp is the weighting function of CO for the given retrieval (in $ppbv \cdot ppbv^{-1}$) and $profileCO^{4A}$ is the profile used as input in 4A for every simulation. $profileCO^{4A}$ corresponds to average CO conditions: it is constant, equals to 97 ppbv, from the surface to 584 hPa.

Figure 11 shows the evolution of the day-night difference of qCO^{4A} , on the same period and on the same area as in Fig. 4. Given that only one profile is used as input in 4A, the diurnal signal in Fig. 11 is only due to the diurnal variations of the weighting function. Naturally, the second term of the sum in Eq. 2, ΔqCO , is also dependent on the weighting function. But quantifying the impact of the diurnal variations of the weighting function on this term (thus on qCO) would require to know the "true" profiles of CO corresponding to the passes of the sounder, whether these profiles come from observations or simulations of a chemistry-transport model. That's why here we only focus on the day-night difference of qCO^{4A} , which gives an approximation of the influence of the weighting functions, and which can be compared to the diurnal signal of CO in Fig. 4.

As expected, the signal is positive and has almost the same seasonality as the diurnal signal shown in Fig. 4, with a shift of one month. It is about 5 ppbv between December and April, which coarsely corresponds to the bias observed in Fig. 4 for these months, April excepted.

~~This result can suggest that the diurnal excess of CO observed when there is no fire just comes from the diurnal variations of the weighting function.~~ In addition, the amplitude of the signal in Fig. 4 is only about 2 ppbv whereas ~~it is 15 ppbv in Fig. 4.~~

~~This first approximation of the impact amplitude of the variation of the vertical sensitivity on the day-night difference of CO suggests 15 ppbv (Fig. 4).~~

In order to evaluate the impact of the choice of the reference profile $profileCO^{4A}$ on the vertical sensitivity and the diurnal signal of CO, we have performed the same analysis as above assuming a profile characterized by enhanced concentration of CO near the surface: 500 ppbv at the surface and 300 ppbv at the first level above the surface (Fig. S2).

The resulting day-night difference of qCO^{4A} obtained using this strongly polluted profile of CO in the retrieval procedure is plotted in Fig. 11 as blue points for each January, April, July and October between 2008 and 2012. As expected, with the polluted profile, the day-night difference of qCO^{4A} is higher than with the reference profile (red curve). However, it is still low compared to the diurnal signal of CO plotted in Fig. 4 (red curve). Moreover, the amplitude of the signal has only increased by less than 1 ppbv despite the very high values of CO assumed near the surface.

We can thus conclude that the diurnal tropospheric excess of CO retrieved from IASI is not decisively influenced by the variations of the vertical sensitivity, and that it is mostly due to the diurnal cycle of fire emissions.

4.2 Hypothesis on the mechanisms explaining the relation between fires and the day-night difference of CO

As exposed in Section 3.3, the diurnal signals of CO and CO₂ are of opposite signs: Chédin et al. (2008) have shown that CO₂ concentrations in the troposphere are higher by night, whereas ~~the~~ we find here that CO concentrations are higher in the daytime. Several factors can explain this sign difference.

As ~~said~~ stated above, CO and CO₂ are emitted during the flaming and the smoldering phases of the combustion, in which their emissions are anti-correlated. The flaming phase favours CO₂ emissions (Lobert and Warnatz, 1993); it is characterized by high temperatures (800°-1200°C) (Pyne et al., 1996) which entail strong uprisings, and is associated with the combustion of the aboveground biomass. So, during the day, in this phase, fires emit large quantities of CO₂ reaching the high troposphere. At the end of the day, the infrared sounder's measurements, which are representative of the high troposphere, allow to observe this accumulation of fire emissions under the tropopause. Conversely, at the beginning of the day, after the emissions have been diluted and before fires start again (or: before the emissions can reach such altitudes), the sounder only observes the background level of CO₂ (Chédin et al., 2005, 2008).

The other phase of the combustion, the smoldering phase, favours CO emissions (Lobert and Warnatz, 1993); it is characterized by lower temperatures (100°-600°C) (Pyne et al., 1996), which contribute to more stable plumes, more prone to be driven by the variability of the boundary layer; it is associated with the combustion of the organic layer. At the end of the day, still active fires lose their efficiency, favouring CO emissions in the smoldering phase (Ward et al., 1996; Kasischke and Bruhwiler, 2003).

The fact that the smoldering phase can last long, with CO plumes staying close to the surface, entails high CO concentrations in the first layers, in particular at night. For example, Ferguson et al. (2003) measured in Alaska extreme CO concentrations at midnight, reaching 27 ppmv, between 0 and 150 m. altitude. These extreme concentrations are the consequence of a very stable boundary layer. Ferguson et al. (2003) observed almost no smoke at about 2000 m. The day after, fires are less active, and the concentrations are much lower, of the order of a ppmv. The extreme concentrations of the previous day were dissipated by the natural convection and advection. Even though this is an example of a boreal forest fire, it highlights the possibility that, while fires can be very active during the day, with emissions reaching the free troposphere, the majority of the smoke is trapped at ~~vey~~ low altitudes at night, and then uplifted in the morning by the natural convection and the pyroconvection.

Figure ~~11~~12 shows the mean boundary layer height in southern Africa, ~~in~~ and South America, between July and November 2008, i.e. during the fire season, calculated from the ECMWF forecasts. The boundary layer ~~behaves the same way during these months, but the maximum of the height, reached in the early afternoon, increases from July to September and then decreases until November.~~ The boundary layer is ~~very~~always low, at about 200 m., between ~~06:00 7:30~~ 7:30 p.m. and ~~03:00 4:30~~ 4:30 a.m. The natural convection is becoming important only after ~~06:00 7:30~~ 7:30 a.m. When IASI passes at ~~09:30~~ 9:30 p.m., ~~nighttime~~ CO emissions ~~happening at night~~ are trapped in the boundary layer, so they are not visible by the sounder, which is sensitive to CO in the mid-troposphere and insensitive to CO close to the surface by night, as shown in Fig. 9. When IASI passes at ~~09:30~~ 9:30 a.m., the trapped CO has been uplifted by natural convection and reaches altitudes to which the sounder is sensitive to CO. In addition, at ~~09:30~~ 9:30 a.m., fires are active again (mostly in the flaming phase of the combustion), with strong vertical movements that can uplift surrounding smokes. As a result, above burning areas, the day-night difference of CO computed from IASI is a positive signal directly related to fire emissions.

These different factors support the hypothesis of the convection of CO emissions in the mid-troposphere in the morning, following their accumulation in the boundary layer during the night. The sign difference between the diurnal signals of CO and CO₂ is the result of the specificity of the two phases of the combustion and of the difference in the sounder's vertical sensitivity to these two gases.

5 Conclusion

The relation between tropical biomass burning emissions and CO has been analysed by interpreting 5 years (2007-2012) of ~~mid~~-tropospheric CO column retrieved from IASI observations by day and by night (~~09:30~~ 9:30 a.m./p.m. LT), and temporal series of burned areas (MODIS) and fire emissions (GFED3.1 and GFAS1.0). Following Chédin et al. (2005, 2008) who related the diurnal signature of CO₂ retrieved from NOAA10/TOVS instruments to fire emissions, we have taken advantage of the fact that IASI overpasses every point twice a day, before and after the maximum of the diurnal cycle of fires, in order to relate directly fires and CO concentrations in the troposphere.

Unlike retrievals by day or by night, the spatio-temporal evolution of the diurnal signal of tropospheric CO as retrieved from IASI, defined here as the day-night difference of CO, is in agreement with the evolution of fires: this differential approach cancels out the background

CO, including plumes due to advective transport from nearby regions, and is only sensitive to the CO related to local fire emissions. A linear relationship is found [over various regions](#) in the [whole tropical region tropics](#) between [the diurnal difference of IASI CO and CO fire emissions from the GFED3.1 inventory and the diurnal difference of IASI CO](#) ($R^2 \sim 0.6$) and [GFAS1.0](#) ($R^2 \sim 0.7$) [inventories](#). For regions near the equator, daytime and nighttime orbits of the sounder overlap less, inducing a limited number of clear-sky spots available.

Some discrepancies arise between [GFED](#) emissions [from GFED3.1 and GFAS1.0](#) and IASI CO in southern Africa [\(i\) in](#). In terms of seasonality: in regions of wooden savannas, the fire activity suggested by the IASI day-night difference of CO is more intense towards the end of the fire season (September) than GFED3.1 [and GFAS1.0](#) emissions indicate. It might be due to the fact that these regions with dense fuel are likely to favour carbon emissions during the smoldering phase up until the end of the fire season; [\(ii\) in](#). In terms of intensity: this could indicate that the specificity of CO emissions compared to CO₂ emissions for each biome might need to be refined in the emission inventory's framework.

The diurnal signals of CO₂ from TOVS (Chédin et al., 2005, 2008) and CO from IASI are of opposite signs. CO retrievals are indeed higher in the daytime than in the nighttime, unlike CO₂ retrievals. The suggested mechanism explaining the diurnal signal of CO is as follows: CO is emitted in large quantities in the smoldering phase of the combustion occurring during the night (after that fires in the flaming phase have burned the above ground vegetation in the daytime), and accumulates in the boundary layer, until being uplifted from the beginning of the day. This hypothesis is supported both by the specificity of CO emissions compared to CO₂ emissions, as well as by the fact that the retrievals of these gases are not representative of the same part of the atmosphere. Simulations with general circulation models should help to validate the plausibility of this mechanism, and to compare the effects of vertical transport patterns related to the different combustion phases on the injection of CO and CO₂ in the mid and upper troposphere. The results presented here show that the analysis of diurnal variations of CO and CO₂ as measured from space can give us a global view of the repartition of the emissions between the flaming and the smoldering phase and of their associated transport, which need to be taken into account in surface flux estimation procedures and emission inventories.

[The monitoring of CO from space with our retrieval method can be extended to IASI observations on Metop-B, which was launched in 2012, and Metop-C, which will be launched in 2017, providing at least 20 years of observations at the same passing times. As part of the EUMETSAT Polar System-Second Generation \(EPS-SG\) program, IASI-New Generation \(IASI-NG, Crevoisier et al., 2014\) will cover the period 2020-2042 on the same orbit as IASI, allowing us to study on the long term the evolution of CO, its diurnal cycle and its relation with fires. Our CO retrieval method can also be applied to Aqua/AIRS observations \(see Thonat et al., 2012\), whose passing times are 1.30 a.m./p.m, giving us four points in the diurnal cycle of CO. CrIs, with the same characteristics as AIRS, was launched in 2011 and will also be on the Joint Polar Satellite System \(JPSS\) program planned for 2017. Since IASI enables the retrieval of other gases emitted by fires such as CO₂ and CH₄, it also gives the opportunity of a multispecies study that can provide a more accurate view of the specificities of fire emissions.](#)

[Acknowledgements.](#) This research was supported by Centre National d'Etudes Spatiales (CNES, France) and Microsoft Research Ltd. This work has also been supported by the

5 [Agence Nationale de la Recherche under contract 2010 BLAN 611 01 “TropFire”. IASI has been developed and built under the responsibility of CNES. It is flown onboard the MetOp satellites as part of the EUMETSAT Polar System. The IASI L1 data are received through the EUMETCast near real time data distribution service. We particularly wish to thank the ETHER centre team for their help in getting IASI data. Calculations were performed using the resources of IDRIS, the computing centre of CNRS, of ECMWF and of the IPSL data and computing centre ClimServ.](#)

10 **References**

15 [Andreae, M. O.: Biomass burning: Its history, use and distribution and its impacts on environmental quality and global climate, in: Global Biomass Burning: Atmospheric, Climatic, and Biospheric Implications, J. S. Levine, MIT Press, Cambridge, 3-21, 1991.](#)

[Andreae, M. O., Rosenfeld, D., Artaxo, P., Costa, A. A., Frank, G. P., Longo, K. M., and Silva-Dias, M. A. F.: Smoking Rain Clouds over the Amazon, Science, 303, 1337-1342, doi: 10.1126/science.1092779, 2004.](#)

20 Barbosa, P. M., Stroppiana, D., Grégoire, J. M., and Pereira, J. M. C.: An assessment of vegetation fire in Africa (1981-1991): burned areas, burned biomass, and atmospheric emissions, *Global Biogeochem. Cycles*, 13, 933-950, 1999.

25 Bowman, D. M. J. S., Balch, J. K., Artaxo, P., Bond, W. J., Carlson, J. M., Cochrane, M. A., D’Antonio, C. M., DeFries, R. S., Doyle, J. C., Harrison, S. P., Johnston, F. H., Keeley, J. E., Krawchuk, M. A., Kull, C. A., Marston, J. B., Moritz, M. A., Prentice, I. C., Roos, C. I., Scott, A. C., Swetnam, T. W., van der Werf, G. R., and Pyne, S. J.: Fire in Earth System, *Science*, 324, 481-484, 2009.

30 Brenninkmeijer, C. A. M., Crutzen, P., Boumard, F., Dauer, T., Dix, B., Ebinghauss, R., Filippi, D., Fischer, H., Franke, H., Frie, U., Heintzenberg, J., Helleis, F., Hermann, M., Kock, H. H., Koeppel, C., Lelieveld, J., Leuenberger, M., Martinsson, B. G., Miemczyk, S., Moret, H. P., Nguyen, H. N., Nyfeler, P., Oram, D., O’Sullivan, D., Penkett, S., Platt, U., Pucek, M., Ramonet, M., Randa, B., Reichelt, M., Rhee, T. S., Rohwer, J., Rosenfeld, K.,
35 Scharffe, D., Schlager, H., Schumann, U., Slemr, F., Sprung, D., Stock, P., Thaler, R., Valentino, F., van Velthoven, P., Waibel, A., Wandel, A., Waschitschek, K., Wiedensohler, A., Xueref-Remy, I., Zahn, A., Zech, U., and Ziereis, H.: Civil Aircraft for the regular investigation of the atmosphere based on an instrumented container: The new CARIBIC system, *Atmos. Chem. Phys.*, 7, 4953-4976, doi:10.5194/acp-7-4953-2007, 2007.

40 Buchwitz, M., Khlystova, I., Bovensmann, H., and Burrows, J. P.: Three years of global carbon monoxide from SCIAMACHY: comparison with MOPITT and first results related to the detection of enhanced CO over cities, *Atmos. Chem. Phys.*, 7, 2399-2411, doi:10.5194/acp-7-2399-2007, 2007.

45 Cahoon, D. R., Stocks, B. J., Levine, J. S., Coter III, W. R., and O’Neill, C. P.: Seasonal distribution of African fires, *Nature*, 359, 812-815, 1992.

- Chédin, A., Serrar, S., Scott, N. A., Pierangelo, C., and Ciais, P.: Impact of tropical biomass burning emission on the diurnal cycle of upper tropospheric CO₂ retrieved from NOAA 10 satellite observations, *J. Geophys. Res.*, 110, D11309, doi:10.1029/2004JD005540, 2005.
- 5 Chédin, A., Scott, N. A., Armante, R., Pierangelo, C., Crevoisier, C., Fossé, O., and Ciais, P.: A quantitative link between CO₂ emissions from tropical vegetation fires and the daily tropospheric excess (DTE) of CO₂ seen by NOAA-10 (1987–1991), *J. Geophys. Res.*, 113, D05302, doi:10.1029/2007JD008576, 2008.
- 10 Crevoisier, C., Chédin, A., Heilliette, S., Scott, N. A., Serrar, S., Armante, R.: Mid-tropospheric CO₂ retrieval in the tropical zone from AIRS observations, *Proceedings of the 13th International TOVS Study Conference*, 2003.
- 15 [Crevoisier, C., Clerbaux, C., Guidard, V., Phulpin, T., Armante, R., Barret, B., Camy-Peyret, C., Chaboureau, J.-P., Coheur, P.-F., Crépeau, L., Dufour, G., Labonnote, L., Lavanant, L., Hadji-Lazaro, J., Herbin, H., Jacquinet-Husson, N., Payan, S., Péquignot, E., Pierangelo, C., Sellitto, P., and Stubenrauch, C.: Towards IASI-New Generation \(IASI-NG\): impact of improved spectral resolution and radiometric noise on the retrieval of thermodynamic, chemistry and climate variables, *Atmos. Meas. Tech.*, 7, 4367-4385, doi:10.5194/amt-7-4367-2014, 2014.](#)
- 20
- Duncan, B. N., Martin, R. V., Staudt, A. C., Yevich, R., and Logan, J. A.: Interannual and seasonal variability of biomass burning emissions constrained by satellite observations, *J. Geophys. Res.*, 108(D2), 4100, doi:10.1029/2002JD002378, 2003.
- 25
- Duncan, B. N., Logan, J. A., Bey, I., Megretskaia, I. A., Yantosca, R. M., Novelli, P. C., Jones, N. B., and Rinsland, C. P.: Global budget of CO, 1988-1997: Source estimates and validation with a global model, *J. Geophys. Res.*, 112, D22301, doi:1029/2007JD008459, 2007.
- 30
- Edwards, D. P., Emmons, L. K., Gille, J. C., Chu, A., Attié, J.-L., Giglio, L., Wood, S. W., Haywood, J., Deeter, M. N., Massie, S. T., Ziskin, D. C., and Drummond, J. R.: Satellite-observed pollution from Southern Hemisphere biomass burning, *J. Geophys. Res.*, 111, D14312, doi:10.1029/2005JD006655, 2006.
- 35
- Engelstaedter, S., Tegen, I., Washington, R.: North African dust emissions and transport, *Earth-Sc. Rev.*, 79, 73-100, 2006.
- Ferguson, S. A., Collins, R. L., Ruthford, J., and Fukuda, M.: Vertical distribution of nighttime smoke following a wildland biomass fire in boreal Alaska, *J. Geophys. Res.*, 108, 4743, doi:10.1029/2002JD003324, 2003.
- 40
- 45 [Freeborn, P. H., Wooster, M. J., Hao, W. M., Ryan, C. A., Nordgren, B. L., Baker, S. P., and Ichoku, C.: Relationships between energy release, fuel mass loss, and trace gas and aerosol emissions during laboratory biomass fires, *J. Geophys. Res.*, 113, D01301, doi:10.1029/2007JD008679, 2008.](#)
- Freitas, S. R., Longo, K. M., and Andreae, M. O.: Impact if including the plume rise of vegetation fires in numerical simulations of associated atmospheric pollutants, *Geophys. Res. Lett.*, 33, L17808, doi:10.1029/2006GL026608, 2006.
- 50

- Giglio, L.: Characterization of the tropical diurnal fire cycle using VIRS and MODIS observations. *Remote Sens. Environ.*, 108, 407-421, doi:10.16/j.rse.2006.11.018, 2007.
- 5 Guan, H., Chatfield, R. B., Freitas, S. R., Bergstrom, R. W., and Longo, K. M.: Modeling the effect of plume-rise on the transport of carbon monoxide over Africa with NCAR CAM, *Atmos. Chem. Phys.*, 8, 6801-6812, doi:10.5194/acp-8-6801-2008, 2008.
- 10 Hilton, F., Armante, R., August, T., Barnet, C., Bouchard, A., Camy-Peyret, C., Capelle, V., Clarisse, L., Clerbaux, C., Coheur, P.-F., Collard, A., Crevoisier, C., Dufour, G., Edwards, D., Faijan, F., Fourrié, N., Gambacorta, A., Goldberg, M., Guidard, V., Hurtmans, D., Illingworth, S., Jacquinet-Husson, N., Kerzenmacher, T., Klaes, D., Lavanant, L., Masiello, G., Matricardi, M., McNally, A., Newman, S., Pavelin, E., Payan, S., Péquignot, E., Peyridieu, S., Phulpin, T., Remedios, J., Schlüssel, P., Serio, C., Strow, L., Stubenrauch, C.,
15 Taylor, J., Tobin, D., Wolf, W., Zhou, D., Hyperspectral Earth Observation from IASI: four years of accomplishments, *B. Am. Meteorol. Soc.*, 93, 347-370, doi:10.1175/BAMS-D-11-00027.1, 2012.
- 20 Hoelzemann, J. J., Schultz, M. G., Brasseur, G. P., Granier, C., and Simon, M.: Global Wildland fire Emission Model (GWEM): Evaluating the use of global area burnt satellite data, *J. Geophys. Res.*, 109, D14S04, doi:10.1029/2003JD003666, 2004.
- 25 [Hoelzemann, J. J.: Global Wildland Fire Emission Modeling for Atmospheric Chemistry Studies, Ph.D. thesis, Max Planck Institute for Meteorology/University of Hamburg, Germany, Reports 5 on Earth System Science, 28/2006, ISSN 1614-1199, 2006.](#)
- Holloway, T., Levy II, H., Kasibhatla, P.: Global distribution of carbon monoxide, *J. Geophys. Res.*, 105, 12,123-12,147, 2000.
- 30 IPCC: Climate Change 2007: The Physical Science Basis. Contribution of Working Group I to the Fourth Assessment Report of the Intergovernmental Panel on Climate Change [Solomon, S., D. Qin, M. Manning, Z. Chen, M. Marquis, K.B. Averyt, M.Tignor and H.L. Miller (eds.)], Cambridge University Press, Cambridge, United Kingdom and New York, NY, USA, 2007.
- 35 [Ito, A. and Penner, J. E.: Global estimates of biomass burning emissions based on satellite imagery for the year 2000, J. Geophys. Res., 109, D14S05, doi:10.1029/2003JD004423, 2004.](#)
- 40 Jain, A. K., Tao, Z., Yang, X., Gillespie, C.: Estimates of global biomass burning emissions for reactive greenhouse gases (CO, NMHCs, and NO_x) and CO₂, *J. Geophys. Res.*, 111, D06304, doi:10.1029/2005JD006237, 2006.
- 45 [Kaiser, J. W., Heil, A., Andreae, M. O., Benedetti, A., Chubarova, N., Jones, L., Morcrette, J.-J., Razinger, M., Schultz, M. G., Suttie, M., and van der Werf, G. R.: Biomass burning emissions estimated with a global fire assimilation system based on observed fire radiative power, *Biogeosc.*, 9, 527-554, 2012.](#)

- Kasischke, E. S., and Bruhwiler, L. P.: Emissions of carbon dioxide, carbon monoxide, and methane from boreal forest fires in 1998, *J. Geophys. Res.*, 108, 8146, doi:10.1029/2001JD000461, 2003.
- 5 Langenfelds, R. L., Francey, R. J., Pak, B. C., Steele, L. P., Llyod, J., Trudinger, C. M., and Allison, C. E.: Interannual growth rate variations of atmospheric CO₂ and its $\delta^{13}\text{C}$, H₂, CH₄, and CO between 1992 and 1999 linked to biomass burning, *Global Biogeochem. Cycles*, 16(3), 1048, doi:10.1029/2001GB001466, 2002.
- 10 Lavoué, D., Liousse, C., Cahier, H., Stocks, B. J., and Goldammer, J. G.: Modeling of carbonaceous particles emitted by boreal and temperate wildland fires at northern latitudes, *J. Geophys. Res.*, 105(D22), 26, 871-26,890, 2000.
- 15 Lehsten, V., Tansey, K., Balzter, H., Thonicke, K., Spessa, A., Weber, U., Smith, B., and Arneth, A.: Estimating carbon emissions from African wildfires, *Biogeosci.*, 6, 349-360, 2009.
- Lobert, J. M., and Warnatz, J.: Emissions from the combustion process in vegetation, in: *Fire in the environment: The ecological, atmospheric, and climatic importance of vegetation fires*, Crutzen, P. J., and Goldammer, J. G., Wiley, Chichester, 15-37, 1993.
- 20 Mayaux, P., Bartholome, E. M. C., Eva, H. D., Van Custem, C., Cabral, A., Nonguierma, A., Diallo, O., Pretorius, C., Thompson, M., Cherlet, M., Pekel, J.-F., Defourny, P., Vasconcelos, M., Di Gregorio, A., Fritz, S., De Grandi, G., Elvidge, C., Vogt, P., and Belward, A. S.: A Land Cover Map of Africa. Carte de l'Occupation du Sol de l'Afrique, European Commission, JRC24914, 2003.
- 25 McMillan, W. W., Barnet, C., Strow, L., Chahine, M. T., McCourt, M. L., Warner, J. X., Novelli, P. C., Korontzi, S., Maddy, E. S., and Datta, S.: Daily global maps of carbon monoxide from NASA's Atmospheric Infrared Sounder, *Geophys. Res. Lett.*, 32, L11801, doi:10.1029/2004GL021821, 2005.
- 30 McMillan, W. W., Warner, J. X., McCourt Comer, M., Maddy, E., Chu, A., Sparling, L., Eloranta, E., Hoff, R., Sachse, G., Barnet, C., Razenkov, I., and Wolf, W.: AIRS views transport from 12 to 22 July 2004 Alaskan/Canadian fires: Correlation of AIRS CO and MODIS AOD with forward trajectories and comparison of AIRS CO retrievals with DC-8 in situ measurements during INTEX-A/ICARITT, *J. Geophys. Res.*, 113, D20301, doi:10.1029/2007JD009711, 2008.
- 35 Pierangelo, C., Chédin, A., Heilliette, S., Jacquinet-Husson, N., and Armante, R.: Dust altitude and infrared optical depth from AIRS, *Atmos. Chem. Phys.*, 4, 1813-1822, doi:10.5194/acp-4-1813-2004, 2004.
- 40 Pyne, S. J., Andrews, P. L., and Laven, R. D., *Introduction to Wildland Fire*, 2nd edn., John Wiley, New-York, 14-25, 1996.
- 45 Rio, C., Hourdin, F., and Chédin, A.: Numerical simulation of tropospheric injection of biomass burning products by pyro-thermal plumes, *Atmos. Chem. Phys.*, 10, 3463-3478, doi:10.5194/acp-10-3463-2010, 2010.

- Roberts, G., Wooster, M. J., and Lagoudakis, E.: Annual and diurnal African biomass burning temporal dynamics, *Biogeosc.*, 6, 849-866, doi:5194/bg-6-849-2009, 2009.
- Roy, D. P., Boschetti, L., Justice, C. O., and Ju, J.: The collection 5 MODIS burnt area product – Global evaluation by comparison with the MODIS active fire product, *Remote Sens. Environ.*, 112, 3690-3707, 2008.
- Spivakovsky, C. M., Yevich, R., Logan, J. A., Wofsy, S. C., McElroy, M. B., and Prather, M. J.: Tropospheric OH in a three-dimensional chemical tracer model: An assessment based on observations of CH₃CCl₃, *J. Geophys. Res.*, 95, 18,441-18,471, 1990.
- [Schultz, M. G., Heil, A., Hoelzemann, J. J., Spessa, A., Thonicke, K., Goldammer, J. G., Held, A. C., Pereira, J. M. C., and van het Bolscher, M.: Global wildland fire emissions from 1960 to 2000, *Global Biogeochem. Cy.*, 22, GB2002, doi:10.1029/2007GB003031, 2008.](#)
- Scott, N. A., and Chédin, A.: A fast line-by-line method for atmospheric absorption computations: The Automated Atmospheric Absorption Atlas, *J. Appl. Meteor.*, 20, 802-812, 1981.
- Seiler, W., and Crutzen, P. J.: Estimates of gross and net fluxes of carbon between the biosphere from biomass burning, *Clim. Change*, 2, 207-247, 1980.
- Streets, D. G., Zhang, Q., Wang, L., He, K., Hao, J., Wu, Y., Tang, Y., and Carmichael, G. R.: Revisiting China's CO emissions after Transport and Chemical Evolution over the Pacific (TRACE-P) mission: Synthesis of inventories, atmospheric modeling, and observations, *J. Geophys. Res.*, 111, D14306, doi:10.1029/2006JD007118, 2006.
- Thonat, T., Crevoisier, C., Scott, N. A., Chédin, A., Schuck, T., Armante, R., and Crépeau, L.: Retrieval of tropospheric CO column from hyperspectral infrared sounders – application to four years of Aqua/AIRS and MetOp-A/IASI, *Atmos. Meas. Tech.*, 5, 2413-2429, doi:10.5194/amt-5-2413-2012, 2012.
- Turquety, S., Logan, J. A., Jacob, D. J., Hudman, R. C., Leung, F. Y., Heald, C. L., Yantosca, R. M., Wu, S., Emmons, L. K., Edwards, D. P., and Sachse, G. W.: Inventory of boreal fire emissions for North America in 2004: Importance of peat burning and pyroconvective injection, *J. Geophys. Res.*, 112, D12S03, doi:10.1029/2006JD007281, 2007.
- Turquety, S., Hurtmans, D., Hadji-Lazaro, J., Coheur, P. F., Clerbaux, C., Josset, C., and Tsamalis, C.: Tracking the emission and transport from wildfires using the IASI CO retrievals: analysis of the summer 2007 Greek fires, *Atmos. Chem. Phys.*, 9, 4897-4913, doi:10.5194/acp-9-4897-2009, 2009.
- van der Werf, G. R., Randerson, J. T., Giglio, L., Collatz, G. J., Kasibhatla, P. S., and Arellano, A. F.: Interannual variability in global biomass burning emissions from 1997 to 2004, *Atmos. Chem. Phys.*, 6, 3423-2441, doi:10.5194/acp-6-3423-2006, 2006.
- van der Werf, G. R., Randerson, J. T., Giglio, L., Collatz, G. J., Mu, M., Kasibhatla, P. S., Morton, D. C., DeFries, R. S., Jin, Y., and van Leeuwen, T. T.: Global fire emissions and contribution of deforestation, savanna, forest, agricultural, and peat fires (1997-2009), *Atmos. Chem. Phys.*, 10, 11707-11735, doi:10.5194/acp-10-11707-2010, 2010.

Ward, D. E., Hao, W. M., Susott, R. A., Babitt, R. E., Shea, R. W., Kauffman, J. B., and Justice, C. O.: Effect of fuel composition efficiency and emission factors for African savanna ecosystems, *J. Geophys. Res.*, 101, 23569-23576, 1996.

5

[Wooster, M. J., Roberts, G., Perry, G. L. W., and Kaufman, Y. J.: Retrieval of biomass combustion rates and totals from fire radiative power observations: FRP derived and calibration relationships between biomass consumption and fire radiative energy release, *J. Geophys. Res.*, 110, D24311, di:10.1029/2005JD006318, 2005.](#)

10

Yurganov, N. L., McMillan, W. W., Dzhola, A. V., Grechko, E. I., Jones, N. B., and van der Werf, G. R.: Global AIRS and MOPITT CO measurements: Validation, comparison, and links to biomass burning variations and carbon cycle, *J. Geophys. Res.*, 113, D09301, doi:10.1029/2007JD009229, 2008.

15

Yurganov, L. N., Rakitin, V., Dzhola, A., August, T., Fokeeva, E., George, M., Gorchakov, G., Grechko, E., Hannon, S., Karpov, A., Ott, L., Semutnikova, E., Shumsky, R., and Strow, L.: Satellite- and ground-based CO total column observations over 2010 Russian fires: accuracy of top-down estimates based on thermal IR satellite data, *Atmos. Chem. Phys.*, 11, 7925-7942, doi:10.5194/acp-11-7925-2011, 2011.

20

25

30

35

40

45

50

Code	Latitude	Longitude
H1	0°S-6°S	8°E-28°E
H2	0°S-6°S	28°E-43°E
H3	6°S-10°S	10°E-28°E
H4	6°S-10°S	28°E-40°E
H5	10°S-14°S	10°E-28°E
H6	10°S-14°S	28°E-43°E
H7	14°S-25°S	10°E-20°E
H8	14°S-25°S	20°E-28°E
H9	14°S-25°S	28°E-40°E
H10	12°S-25°S	42°E-50°E

Table 1. Limits in latitudeLatitudes and longitudelongitudes of the studied areas in southern Africa, corresponding to Fig. 4.

Code	Latitude	Longitude	Code	Latitude	Longitude
AfNW	0°N -15°N-0°N	20°W-20°E	AfSE	0°S-20°S	25°E-40°E
AfNE	0°N -15°N-0°N	30°E-45°E	AfSt	0°S-25°S	10°E-40°E
AfNEC	0°N -15°N-0°N	20°E-45°E	Aft	25°N-25°S	20°W-43°E
AfN	0°N -15°N-0°N	20°W-45°E	AmSE	0°S-25°S	60°W-35°W
AfNt	0°N -25°N-0°N	20°W-45°E	AmC	0°N -25°N-0°N	110°W-62°W
AfSW	0°S-20°S	10°E-25°E	Aus	12°S-25°S	110°E-160°E

Table 2. Limits in latitudeLatitudes and longitudelongitudes of the studied areas in the tropics, corresponding to Fig. 6. Af, Am, Aus respectively stand for Africa, America, Australia. N, S, E, W, respectively stand for North, South, East, West, and t stands for total.

5

10

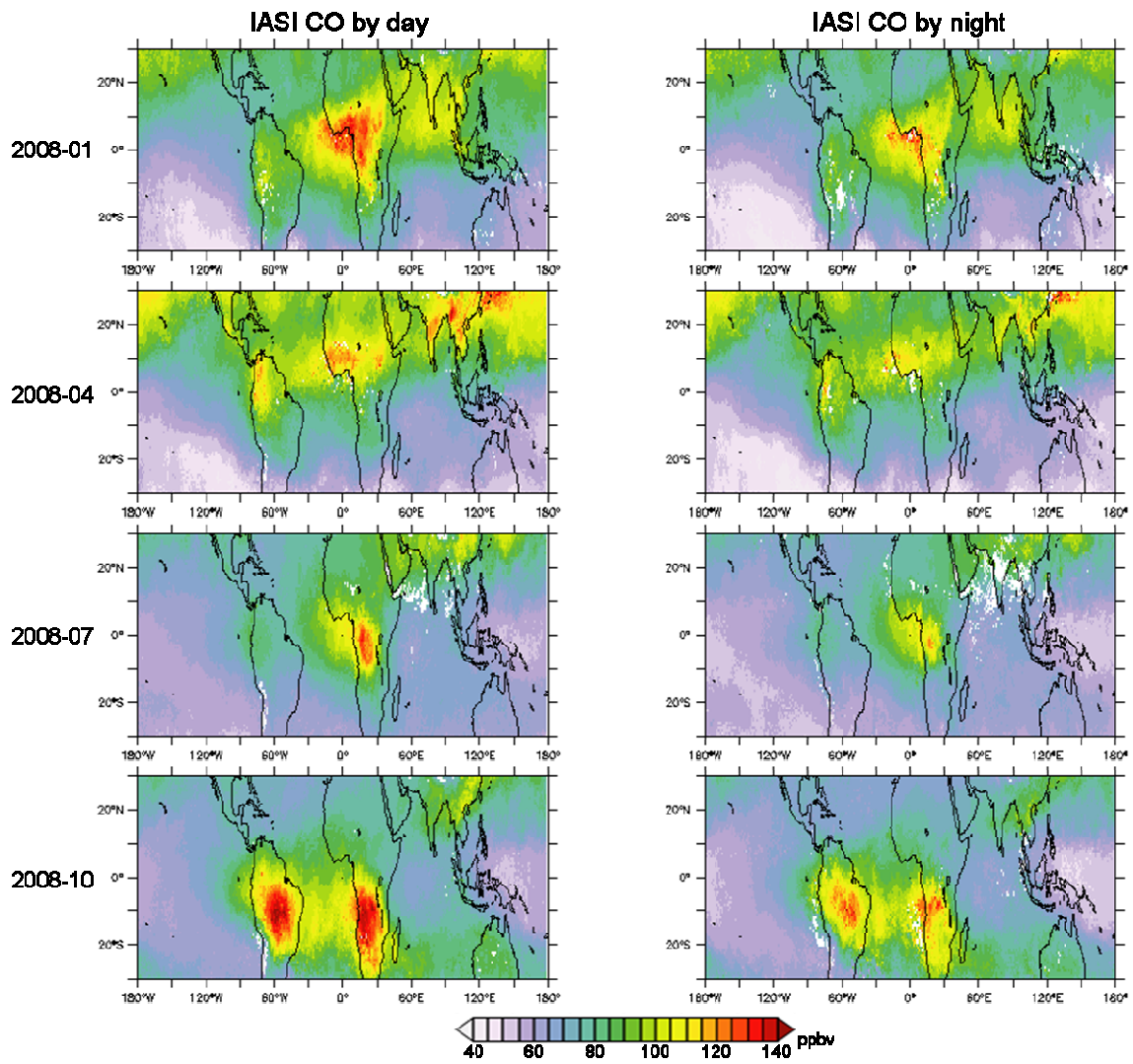
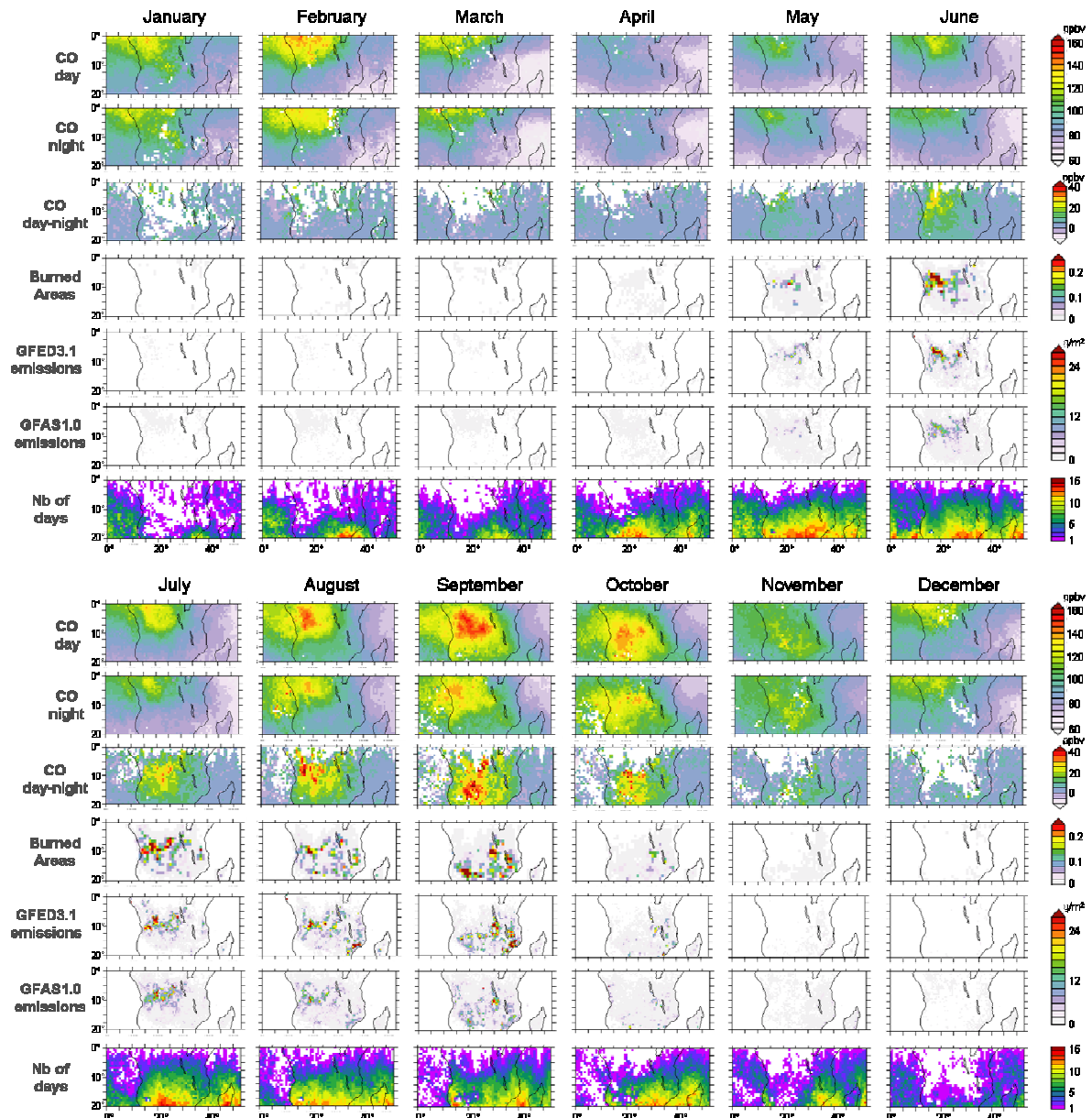


Figure 1. Monthly means of the integrated content of CO from IASI (ppbv), by day (9:30 a.m.) (left) and by night (9:30 p.m.) (right), in January, April, July and October 2008, in the tropics.



5 **Figure 2.** IASI CO and fires between January and December 2008, in southern Africa. (a) From top to bottom: Monthly means of the integrated content of CO from IASI, by day (9:30 a.m.) (in ppbv); by night (9:30 p.m.) (in ppbv); monthly means of the day-night differences of the integrated content of CO from IASI (in ppbv); MODIS Burned Areas (Roy et al., 2008) (in %); GFED3.1 CO emissions (in $\text{g}\cdot\text{m}^{-2}$); GFAS1.0 CO emissions (in $\text{g}\cdot\text{m}^{-2}$); number of days for which the CO day-night difference is available.

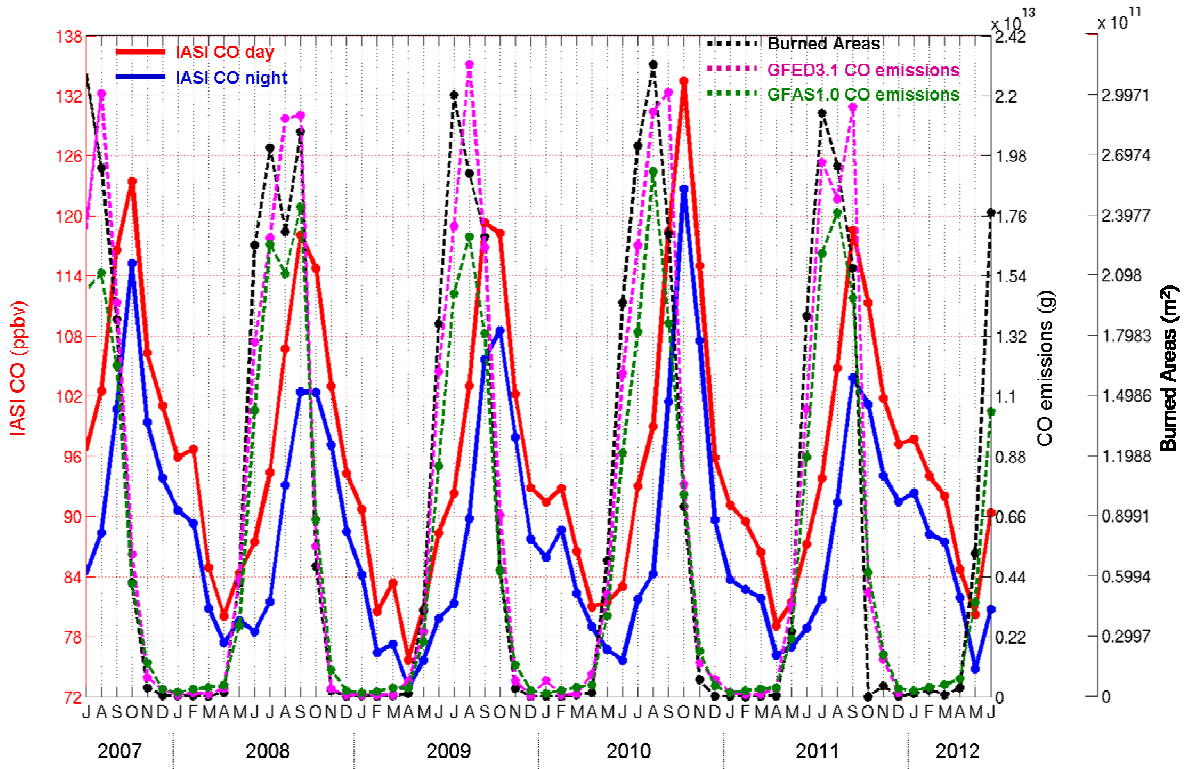


Figure 3. Evolution of the integrated content of CO from IASI on land and of fires between July 2007 and June 2012 in southern Africa ([area comprised between 0°-20°S and, 0° in latitudes, and 0° and °-53°E in longitudes.](#)). Red: CO by day (9:30 a.m.). Blue: CO by night (9:30 p.m.). Black dashed: MODIS Burned Areas. Purple dashed: CO emissions from GFED3.1. [Green dashed: CO emissions from GFAS1.0.](#)

5

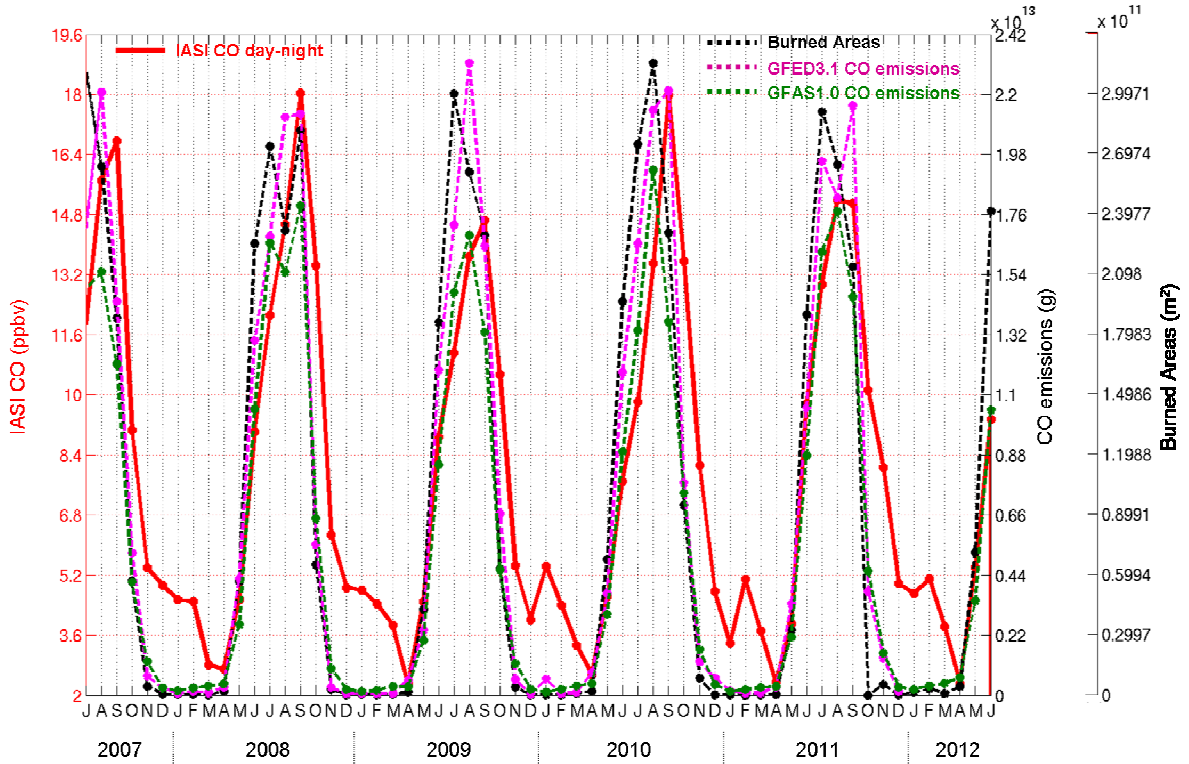


Figure 4. Evolution of the day-night difference of the integrated content of CO from IASI on land, and of fires, between July 2007 and June 2012 in southern Africa. Red: day-night CO. [Blue : CO by night \(09:30 p.m.\)](#). Black dashed: MODIS Burned Areas. Purple dashed: CO emissions from GFED3.1. [Green dashed: CO emissions from GFAS1.0.](#)

10

10 areas in southern Africa and land-cover type

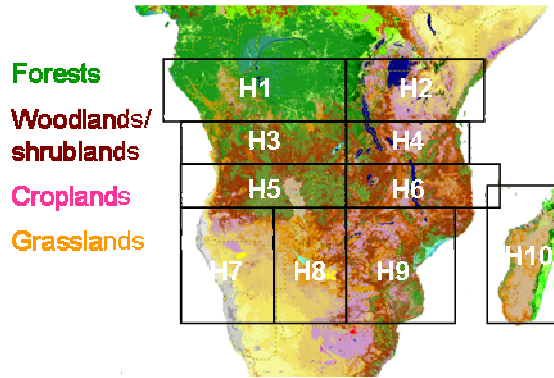


Figure 5. Definition of the studied areas in Africa. (a) Areas in Africa, adapted from Hoelzemann, (2006). (b) Kinds of vegetation, adapted. Vegetation map is from Mayaux et al. (2003).

5

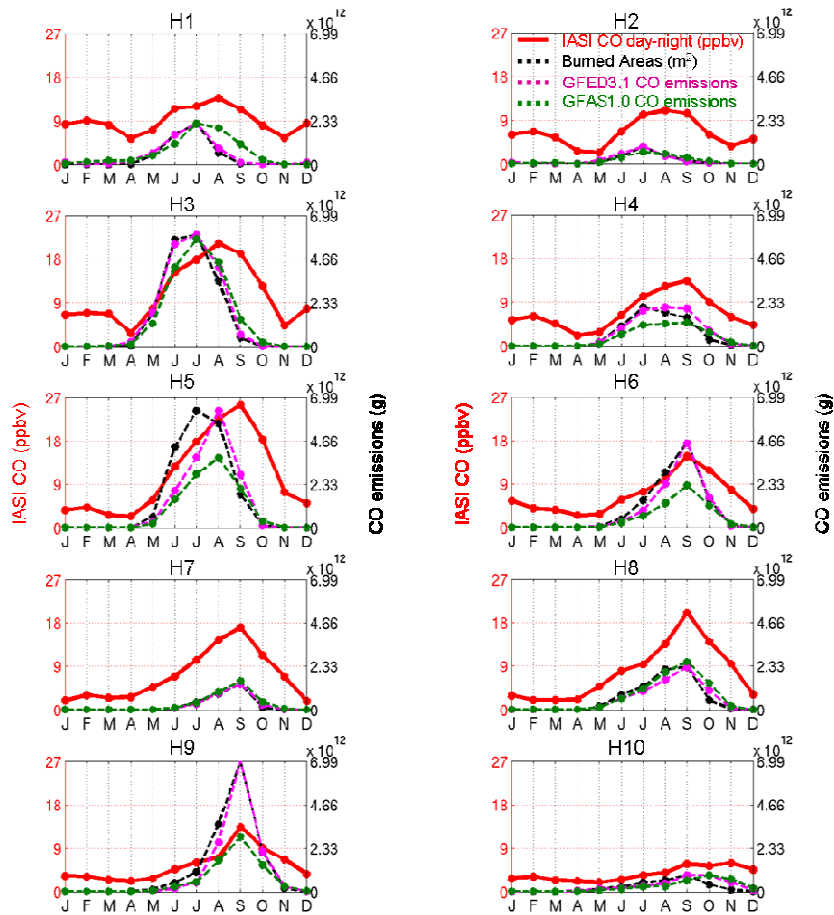


Figure 6. Evolution of the day-night difference of the integrated content of CO from IASI on land, and of fires, on average over 2008-2011 on different areas in southern Africa (see Fig. 5). Red: day-night CO. Black dashed: MODIS Burned Areas. Purple dashed: CO emissions from GFED3.1. Green dashed: CO emissions from GFAS1.0.

10

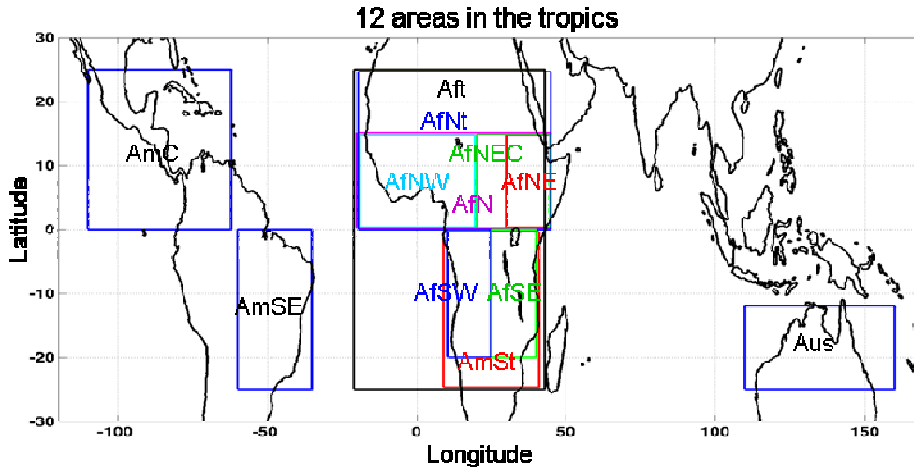


Figure 7. Definition of the studied areas in the tropics. Adapted from Chédin et al. (2008). Only lands are considered. Af, Am, Aus respectively stand for Africa, America, Australia. N, S, E, W, respectively stand for North, South, East, West, and t stands for total.

5

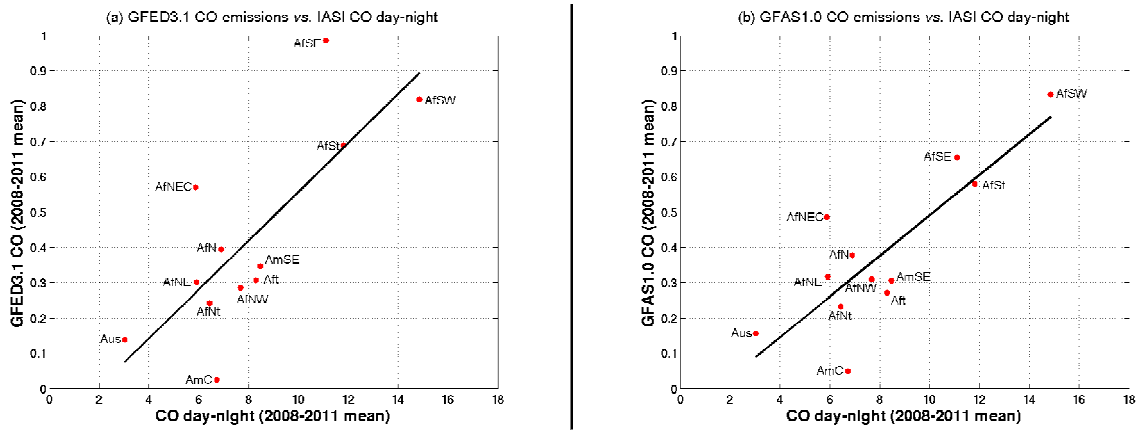
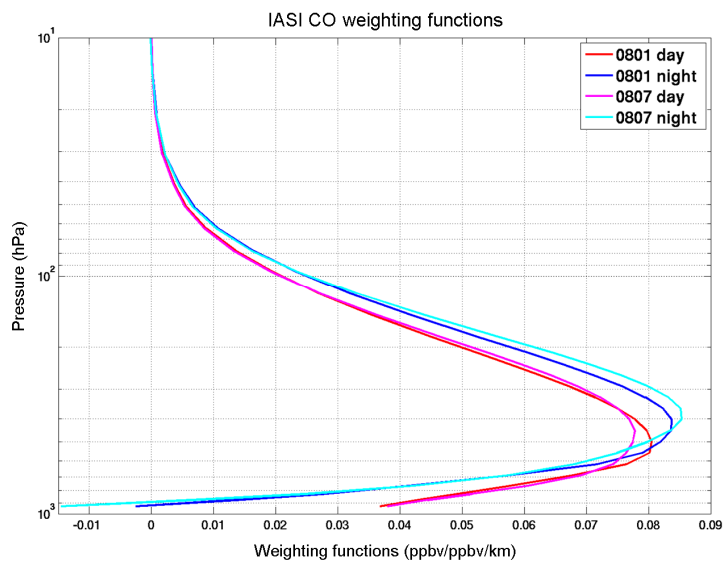


Figure 8. (a) GFED3.1 and (b) GFAS1.0 emissions (in $\text{gCO}\cdot\text{m}^{-2} \times 16$; see text section 3.3) as a function of the day-night difference of the integrated content of CO from IASI (in ppbv) in different tropical areas (see Fig. 7). On average over 2008-2011.



10

Figure 9. IASI CO weighting functions ($\text{ppbv}\cdot\text{ppbv}^{-1}\cdot\text{km}^{-1}$), averaged over southern Africa, on land. Red: January by day (9:30). Blue: January by night (21:30). Magenta: July by day. Cyan: July by night.

IASI CO vs. thermal contrast

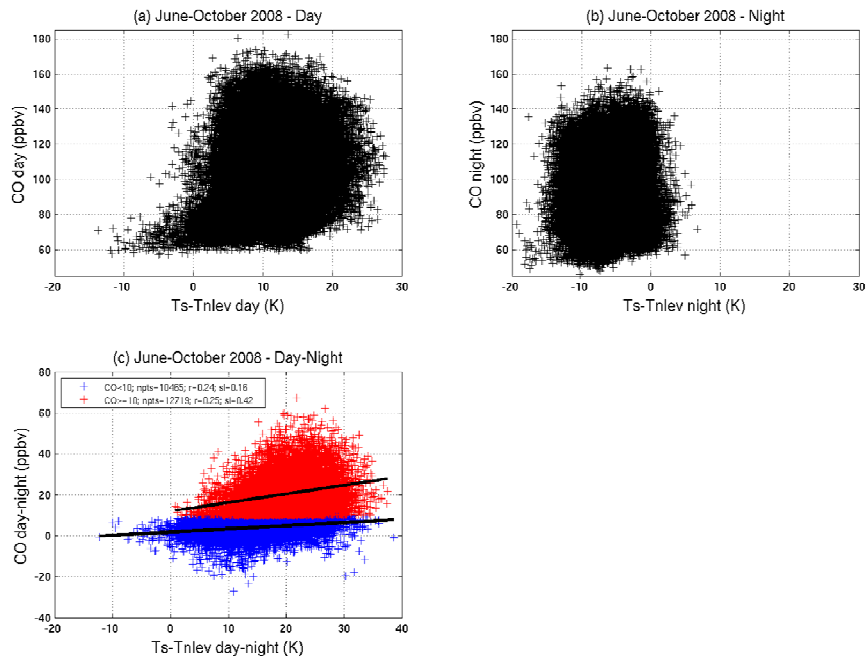


Figure 10. (a) IASI CO (in ppbv) by day as a function of the thermal contrast (in K), between June and October 2008, in southern Africa, on land. (b) Same as (a), by night. (c) Same as (a), for the day-night difference.

5

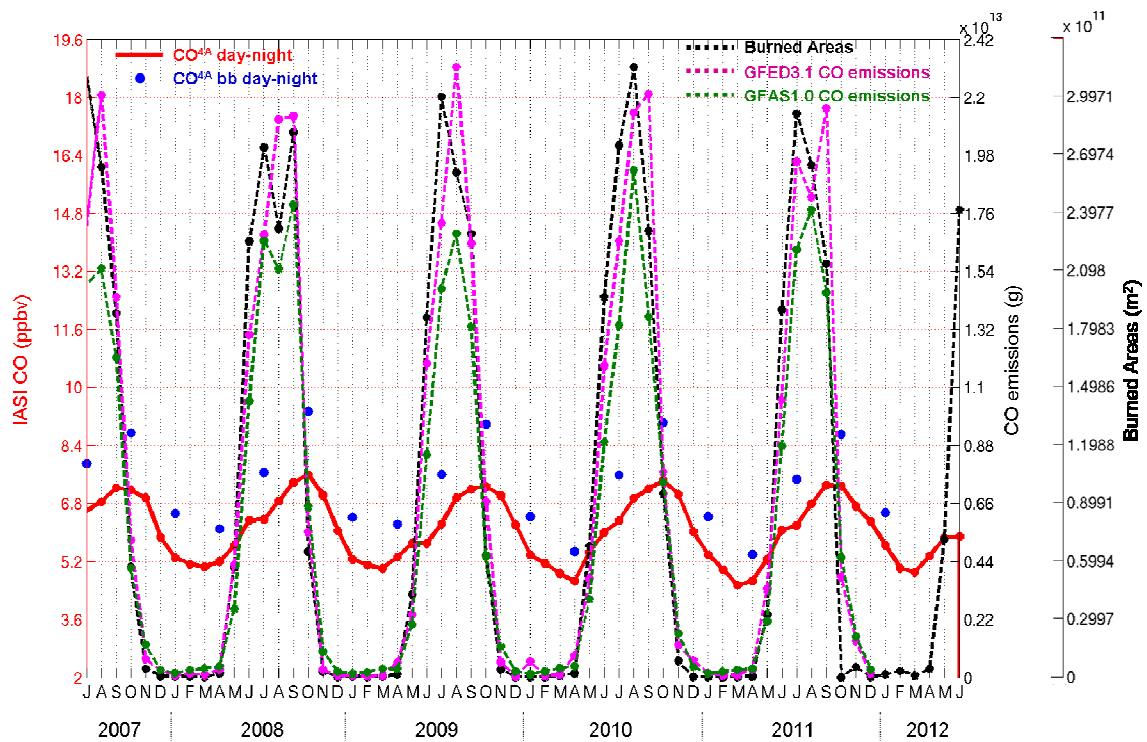
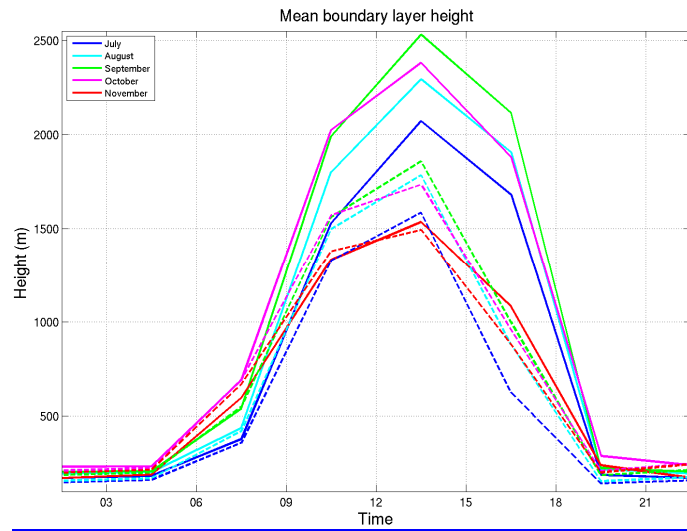


Figure 11. Evolution of the day-night difference of the integrated content qCO^{4A} (see text Sect. 4.1) on land, and of fires, between July 2007 and June 2012 in southern Africa. Red: day-night difference of qCO^{4A} . Blue dots: day-night difference of qCO^{4A} computed with a polluted CO profile as input in 4A. Black dashed: MODIS Burned Areas. Purple dashed: CO emissions from GFED3.1. Green dashed: CO emissions from GFAS1.0.

10



5 **Figure 12.** Mean boundary layer height (solid line) in southern Africa (solid line) and standard deviation South America (dashed lines) between July and November 2008. Plotted from the ECMWF forecasts, which have a 3h time step and a $0.75^{\circ} \times 0.75^{\circ}$ spatial resolution.

10

15

20

25

30

[Supplementary materials](#)

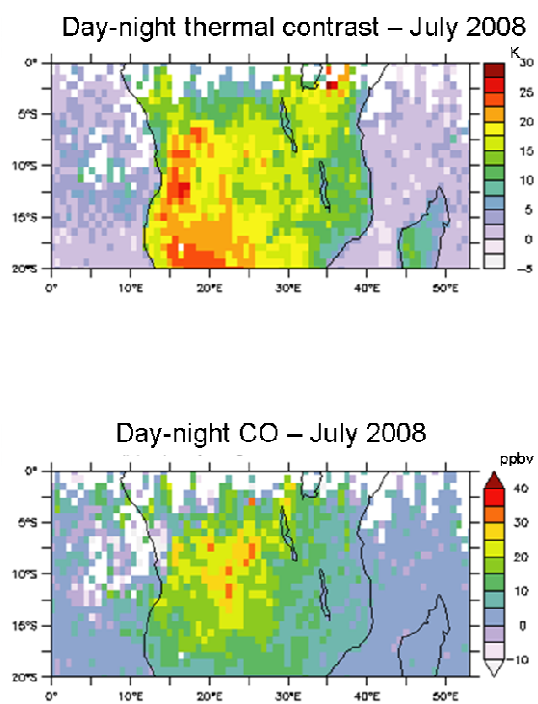


[Figure S1. \(top\) Day-night difference of the thermal contrast \(in K\), in July 2008 in southern Africa. \(bottom\) Day-night difference of IASI CO \(in ppbv\).](#)

5

10

15

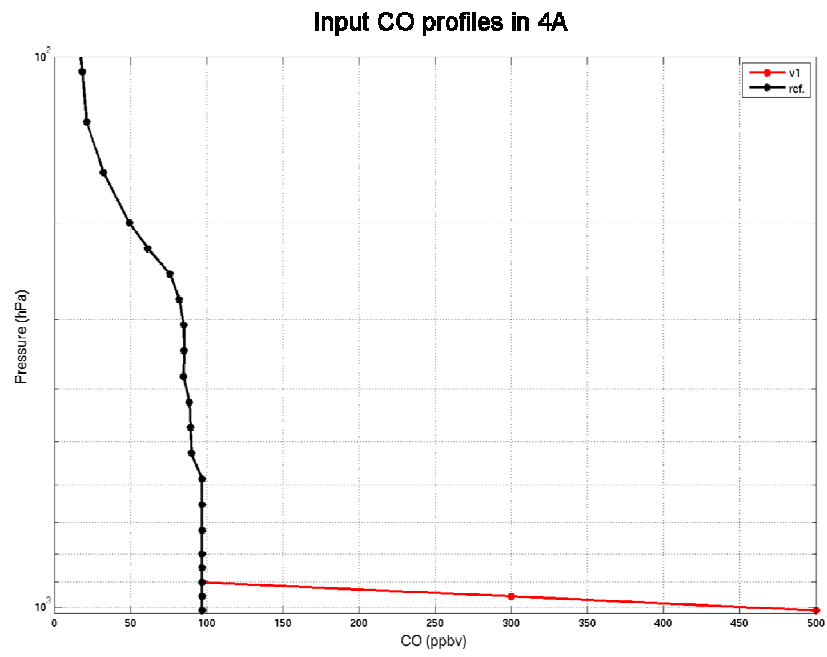


Figure S2. Black: reference profile of CO used as input in 4A for the retrieval of IASI CO (in ppbv). Red: a polluted profile in the boundary layer.